

(12)

ADA 032009

Transition Induced by Distributed Roughness on Blunt Bodies in Supersonic Flow

Nuel

Concepts and Plans Group Directorate
Reentry Systems Division
The Aerospace Corporation
El Segundo, Calif. 90245

409924

29 October 1976

Final Report

APPROVED FOR PUBLIC RELEASE:
DISTRIBUTION UNLIMITED

DDC
RECEIVED
NOV 12 1976
B

Prepared for

SPACE AND MISSILE SYSTEMS ORGANIZATION
AIR FORCE SYSTEMS COMMAND
Los Angeles Air Force Station
P.O. Box 92960, Worldway Postal Center
Los Angeles, Calif. 90009

This final report was submitted by The Aerospace Corporation, El Segundo, CA 90245, under Contract F04701-76-C-0077 with the Space and Missile Systems Organization, Deputy for Reentry Systems, P. O. Box 92960, Worldway Postal Center, Los Angeles, CA 90009. It was reviewed and approved for The Aerospace Corporation by J. F. Mullen, Reentry Systems Division. The project officer was Lt E. G. Taylor, SAMSO (RSSE).

This report has been reviewed by the Information Office (OI) and is releasable to the National Technical Information Service (NTIS). At NTIS, it will be available to the general public, including foreign nations.

This technical report has been reviewed and is approved for publication. Publication of this report does not constitute Air Force approval of the report's findings or conclusions. It is published only for the exchange and stimulation of ideas.

Edward G Taylor
Edward G. Taylor, Lt, USAF
Aeromechanics and Materials
Division
Directorate of Ballistic Systems
Deputy for Reentry Systems

James M. McCormack
James M. McCormack, Major, USAF
Chief, Aeromechanics and
Materials Division
Directorate of Ballistic Systems
Deputy for Reentry Systems

FOR THE COMMANDER

Donald A. Dowler
Donald A. Dowler, Col, USAF
Director, Ballistic Systems
Deputy for Reentry Systems

ACCESSION for		
NTIS	White Section	<input checked="" type="checkbox"/>
DTIC	Diff Section	<input type="checkbox"/>
UNANNOUNCED		<input type="checkbox"/>
JUSTIFICATION.....		
BY.....		
DISTRIBUTION/AVAILABILITY CODES		
Dist.	AVAIL. and/or SPECIAL	
A		

UNCLASSIFIED

SECURITY CLASSIFICATION OF THIS PAGE (When Data Entered)

REPORT DOCUMENTATION PAGE		READ INSTRUCTIONS BEFORE COMPLETING FORM	
1. REPORT NUMBER SAMSO-TR-76-146	2. GOVT ACCESSION NO.	3. RECIPIENT'S CATALOG NUMBER	
4. TITLE (and Subtitle) TRANSITION INDUCED BY DISTRIBUTED ROUGHNESS ON BLUNT BODIES IN SUPERSONIC FLOW.		5. TYPE OF REPORT & PERIOD COVERED Final Rept.	6. PERFORMING ORG. REPORT NUMBER TR-0077(2558-15)-1
7. AUTHOR(s) William M. Bishop	8. CONTRACT OR GRANT NUMBER(s)	F04701-76-C-0077	
9. PERFORMING ORGANIZATION NAME AND ADDRESS The Aerospace Corporation El Segundo, Calif. 90245		10. PROGRAM ELEMENT, PROJECT, TASK AREA & WORK UNIT NUMBERS	
11. CONTROLLING OFFICE NAME AND ADDRESS Space and Missile Systems Organization Air Force Systems Command, LAAFS Los Angeles, California 90009		12. REPORT DATE 29 Oct 1976	13. NUMBER OF PAGES 63 p.
14. MONITORING AGENCY NAME & ADDRESS (if different from Controlling Office)		15. SECURITY CLASS. (of this report) Unclassified	
16. DISTRIBUTION STATEMENT (of this Report) Approved for public release; distribution unlimited.			
17. DISTRIBUTION STATEMENT (of the abstract entered in Block 20, if different from Report)			
18. SUPPLEMENTARY NOTES			
19. KEY WORDS (Continue on reverse side if necessary and identify by block number) Transition Correlation Taylor-Goertler Vortices Distributed Roughnesses Roughness Characterization Supersonic Flow Streamline Curvature Hemispheres, Biconics, Stable Shapes			
20. ABSTRACT (Continue on reverse side if necessary and identify by block number) An empirical model has been developed that correlates transition due to distributed roughnesses, which range in height over five orders of magnitude. The data base is obtained from wind tunnels, arc heaters, and sounding rockets. The shapes included are hemispheres, biconics, and laminar stable. The correlation departs from previous attempts by dividing the body into two distinct regions: a forward region where concave streamline curvature dominates transition, and a following region where streamline			

DD FORM 1473 (FACSIMILE)

409924

UNCLASSIFIED
SECURITY CLASSIFICATION OF THIS PAGE (When Data Entered)

UNCLASSIFIED

SECURITY CLASSIFICATION OF THIS PAGE(When Data Entered)

19. KEY WORDS (Continued)

20. ABSTRACT (Continued)

curvature is not an influence. Noise is found to have little or no effect, and the extension of the correlation to roughnesses measured in micro-inches shows no observable smooth wall limit.

UNCLASSIFIED

SECURITY CLASSIFICATION OF THIS PAGE(When Data Entered)

CONTENTS

I.	INTRODUCTION	3
II.	DISCUSSION	5
	A. Characterization of Roughness	5
	B. The Correlation	6
	C. Comparison With Correlation for 2-D Trips	17
	D. PANT Series J Data	18
	E. 50-MW Arc Data	21
	F. Demetriades, Laderman Data	24
III.	CONCLUSIONS	27
IV.	RECOMMENDATIONS	29
	REFERENCES	31
	NOMENCLATURE	35

TABLES

1.	Collected Transition Data	37
----	-------------------------------------	----

FIGURES

1a.	PANT Data, $M = 5$	9
1b.	NASA-Langley Flight Tests	10
2.	PANT, $M = 5.0$: Correlation of Data in Region of Concave Flow Curvature	12
3.	ART, $M = 7.9$: Correlation of Data in Region of Concave Flow Curvature	14
4.	Additional Wind Tunnel Tests	15
5.	Correlation of Data in Region of Concave Flow Curvature	16
6.	PANT Series J	19
7.	Laminar Blunt - Series J	20
8.	50-MW Arc Data	21
9.	Distribution of Microroughness Characteristics	22
10.	Demetriades, Ladermann Data	23

I. INTRODUCTION

A method for predicting transition has been developed that correlates the effect of distributed roughnesses varying in height over five orders of magnitude. The data base includes the passive nosetip technology (PANT) series A¹ and J², ART³ and various other wind tunnel tests, the NASA-Langley flight tests, and some 50-MW arc data.

The correlation departs from previous attempts by dividing the body into two distinct regions: a forward region where concave streamline curvature in the shock layer dominates transition, and a following region where streamline curvature is not an influence. Noise is found to have little or no effect in most of the experiments, and the extension of the correlation to roughnesses measured in microinches tends to indicate that there is no such thing as a smooth wall.

¹A. D. Anderson, Analysis of PANT Series A Rough Wall Calorimeter Data, Aerotherm Report 73-81, Part II, Aerotherm Division/Acurex Corp., Mountain View, California (1973).

²M. D. Jackson, Interim Report Passive Nosetip Technology (PANT) Program, Aerotherm Report 74-100, Vol. XV, Aerotherm Division/Acurex Corp., Mountain View, California (April 1974).

³R. E. Phinney and F. P. Baltakis, Influence of Roughness on Heat Transfer and Transition: ART Program Data Report, NOLTR 73-231, Naval Ordnance Laboratory, Silver Spring, Maryland (December 1974).

II. DISCUSSION

A. CHARACTERIZATION OF ROUGHNESS

Previous treatments of roughness-induced transition have nondimensionalized roughness height using the "smooth-wall" momentum thickness. Various heuristic arguments on the pros and cons of this approach can be made, but the fact is that it has not produced fully satisfactory correlations. An alternate quantity, the nose diameter ($D = 2R$), has been used here. The basis for this usage is the simple observation that the tripping effectiveness of a roughness element diminishes with the size of the body on which it is placed.

The roughness height used is the peak to valley (PTV) value as suggested by Anderson¹, denoted by k . Several experimenters^{4, 5} have shown that, for distributed three-dimensional roughness elements on blunt bodies, transition occurs at the element or not at all (i. e., disturbances are not amplified downstream as is the case for two-dimensional trips). Thus, in an idealized situation, transition would be distributed about a line determined by the median roughness height. In the actual situation, this picture is modified by the wakes from larger elements that, by obscuring smaller elements, bring transition forward of the median. Thus, for materials with a wide roughness distribution, the approximate line of transition will be determined by those larger elements that occur frequently enough to form such a line. Upstream or downstream departures from this line will occur

⁴ J. B. Peterson and E. A. Horton, An Investigation of the Effect of a Highly Favorable Pressure Gradient on Boundary-Layer Transition as Caused by Various Types of Roughness on a 10-Foot-Diameter Hemisphere at Subsonic Speeds, NASA Memo 2-8-59L, National Aeronautics and Space Administration, Washington, D. C. (April 1959).

⁵ A. E. von Doenhoff and E. A. Horton, A Low-Speed Experimental Investigation of the Effect of a Sandpaper Type of Roughness on Boundary-Layer Transition, Technical Note 3858, National Advisory Committee for Aeronautics, Washington, D. C. (October 1956).

when exceptionally large elements or a region of smaller elements are encountered. This produces transition asymmetries. In this study it was found that the size of the elements that determine this approximate line of transition are those which are shown by a roughness distribution curve, to be greater in height than 85 percent of the elements, k_{85} . This is necessarily an approximate figure and may vary with markedly varying types of roughness. This approach will be discussed in more detail in Section E. For calorimeter tests with a manufactured surface roughness, the distribution is usually quite narrow (intentionally) and the average k approximately equals k_{85} . Thus, the average value of k as reported is used in these cases.

An attempt was made in this analysis to also include roughness spacing in the form of the spacing-to-height ratio λ/k . It was found, however, that λ/k varied at most by a factor of 1.3, while k/D varied by five orders of magnitude and the wall-temperature ratio (to be discussed later) varied by a factor of 3; therefore, no meaningful correlation could be obtained. There may, of course, be other roughness distributions where spacing becomes a factor. The same arguments also apply to individual roughness geometries.

B. THE CORRELATION

In a single PANT transition test, all parameters remained constant except the wall temperature-edge temperature ratio T_w/T_e , which increased with time; this caused transition to move downstream, indicating that an increase in T_w/T_e is stabilizing. In an initial attempt to correct the smooth wall momentum thickness Reynolds number Re_θ to account for this effect, it was observed that the edge Mach number M_e was also a stabilizing influence. These two effects can be rationalized physically in a manner similar to that used by Lees⁶, but using a momentum argument rather than

⁶L. Lees, "Note of the Stabilizing Effect of Centrifugal Forces on the Laminar Boundary Layer Over Convex Surfaces," Journal of the Aeronautical Sciences, 25, 407-408 (June 1958).

considerations of centrifugal acceleration. If a fluid particle near the wall having momentum $\rho_1 u_1$ is displaced outwards towards the boundary layer edge to a point where the momentum is $\rho_2 u_2$, its ability to disturb this flow will be inversely proportional to $\rho_2 u_2 / \rho_1 u_1$ (i.e., a high value of this parameter is stabilizing). For the purposes of this correlation, points 1 and 2 have been taken as the wall and the boundary layer edge, respectively. Of course, directly at the wall $u_1 = 0$ so this term has been replaced by the local speed of sound a_w , which may be regarded as the "disturbance" velocity. Using the equation of state and assuming constant pressure across the boundary layer, this parameter may be written

$$\frac{\rho_e u_e}{\rho_w a_w} \sim \left(\frac{T_w}{T_e} \right)^{1/2} M_e \quad (1)$$

This expression as it stands will produce a satisfactory correction to Re_θ . However, to eliminate the singularity which arises as $Me \rightarrow 0$, this term was included as

$$\left(1 + 4.5 \frac{T_w}{T_e} M_e^2 \right)^{-1/2} \quad (2)$$

where the constants have been determined empirically. With the exception of T_w/T_e , which was not a factor in their experiments, Eq. (2) is similar in form to the correction term obtained empirically by van Driest and Blumer⁷. Thus the value of the term

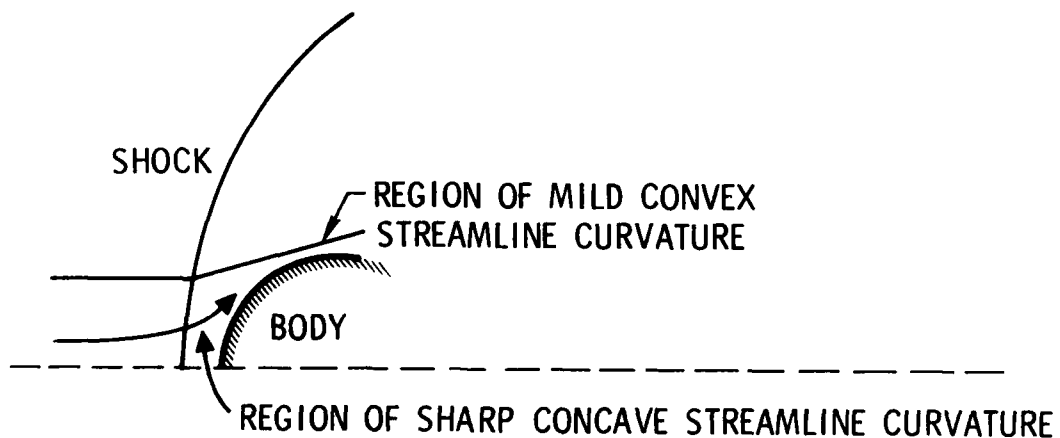
⁷E. R. van Driest and C. B. Blumer, "Boundary-Layer Transition at Supersonic Speeds--Three-Dimensional Roughness Effects (Spheres)," Journal of the Aerospace Sciences, 29, 909-916 (August 1962).

$$\text{Re}_\theta \left(1 + 4.5 \frac{T_w}{T_e} M_e^2 \right)^{-1/2}$$

at transition is shown plotted versus k/D in Figure 1a. All of the PANT data and some of the ART data are shown. The data are extended, by use of the NASA-Langley flight data, down to $10 \mu\text{in.}$ in Figure 1b. Numerical values for all of the data base are given in Table 1. The data fall on or near a line given by

$$\frac{\text{Re}_\theta}{\left(1 + 4.5 \frac{T_w}{T_e} M_e^2 \right)^{1/2}} = 5.6 \left(\frac{k}{D} \right)^{-1/3} \quad (3)$$

with the exception of those points that fall within about 20° of the stagnation point, as indicated on Figure 1b. This latter is the region of concave streamline curvature, which is produced when flow passing through the near-normal portion of the shock must turn sharply to follow the body, as shown below.



It is postulated that this sharp concave flow curvature produces streamwise vortices, known as Goertler vortices, which are destabilizing. A short

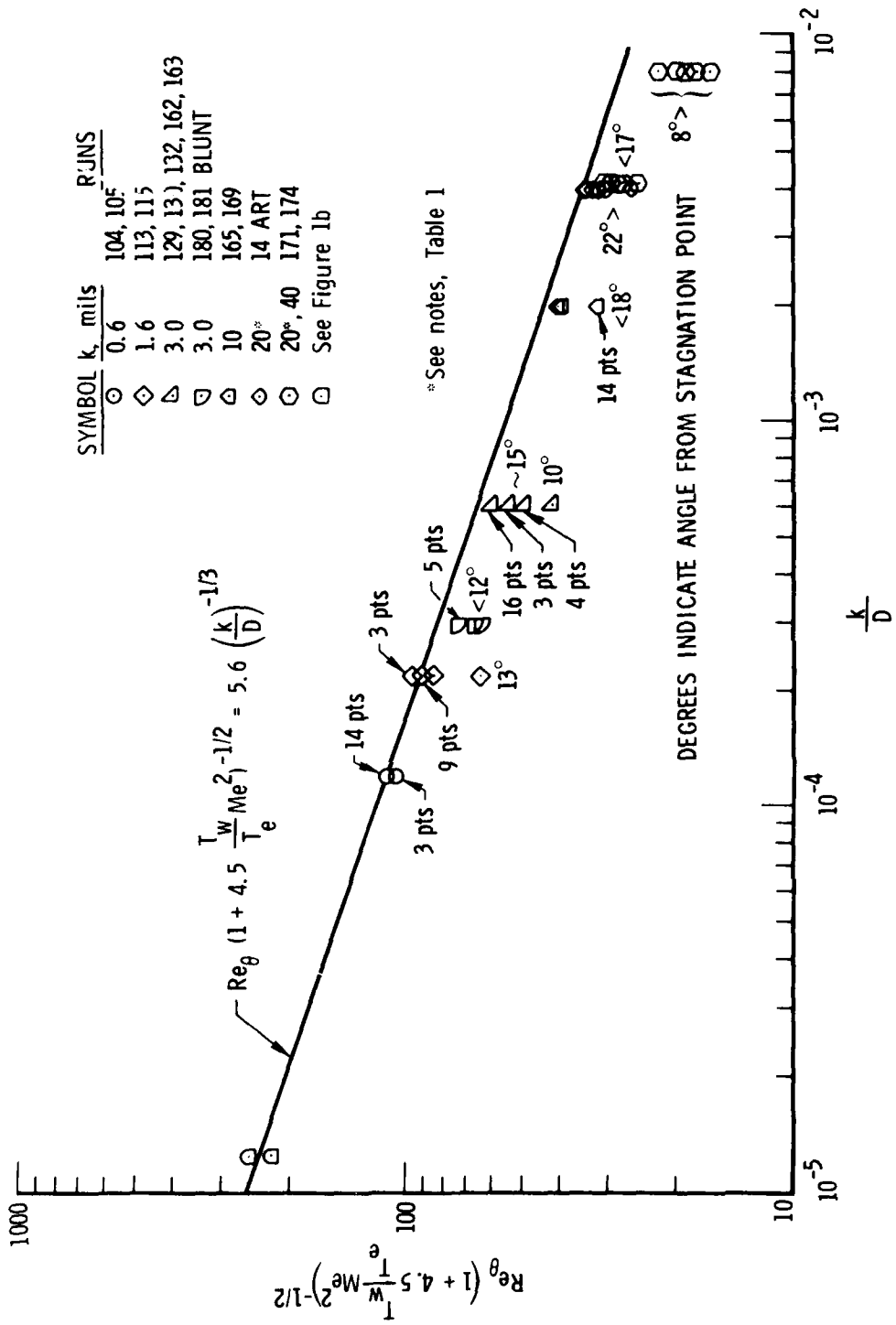
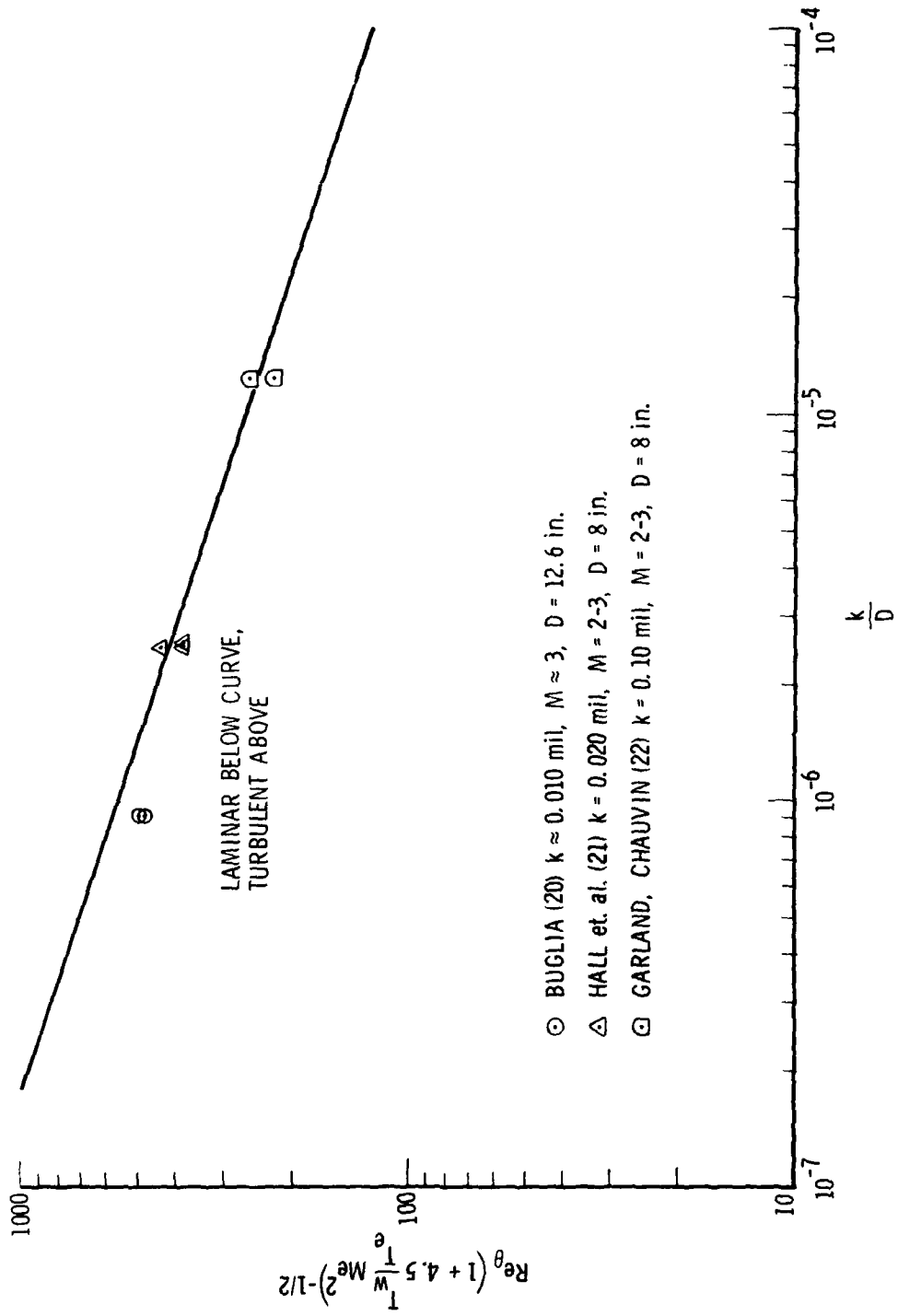


Figure 1a. PANT Data, M = 5



- ⊙ BUGLIA (20) $k \approx 0.010$ mil, $M \approx 3$, $D = 12.6$ in.
- △ HALL et. al. (21) $k = 0.020$ mil, $M = 2-3$, $D = 8$ in.
- ⊖ GARLAND, CHAUVIN (22) $k = 0.10$ mil, $M = 2-3$, $D = 8$ in.

Figure 1b. NASA-Langley Flight Tests

discussion of this phenomenon is given in Schlichting⁸. In particular, Goertler⁹ has calculated that such disturbances exist in the stagnation region of bluff bodies. However, their existence has not yet been empirically demonstrated in a completely satisfactory manner. Whether one believes in vortex formation in the stagnation region or not, it is clear that the nature of the streamline curvature there is radically different from that further back on the nose. This curvature is used here to explain the departure of the forward region transition from that given by Eq. (3). A problem arises in attempting to use curvature as a correlation input, because it is not an easily determined quantity. To avoid this, curvature (and other local flow properties) were assumed to be functions of freestream Reynolds number, $Re_D = U_\infty 2R/\nu$, freestream Mach number, M_∞ , and angle from the stagnation point, S/R . Wall-related parameters were included as before as k/D and T_w/T_e . A correlation of the PANT data for those points only that fall below the curve in Figure 1a is shown in Figure 2. The straight line is given by

$$\left(\frac{T_w}{T_e}\right)^{1.23} \left(\frac{S}{R}\right)^{-1.0} (Re_D)^{-0.6} \left(\frac{k}{D}\right)^{-0.51} = 0.159 \times 10^{-2} \quad (4)$$

Note that this is for constant $M_\infty = 5.0$. At first glance this correlation appears to have considerable scatter, but note that the scales are arithmetic, not logarithmic as in the previous curves. The maximum scatter in this curve is 0.05 radians or an error in transition location of 0.125 in. on the 2.5-in. nose radius PANT test model. This is quite accurate as transition correlations go. A similar plot for the ART data ($M_\infty = 7.9$), i. e., those

⁸H. Schlichting, Boundary-Layer Theory, 6th ed., McGraw-Hill Book Co., New York, pp 500-508 (1968).

⁹H. Görtler, "Dreidimensionale Instabilität der ebenen Staupunktströmung gegenüber wirbelartigen Störungen," Festschrift, Fifty Years of Boundary-Layer Research, Anniversary Volume, eds. H. Görtler and W. Tollmien, Vieweg, Braunschweig, Germany, pp 303-314 (1955).

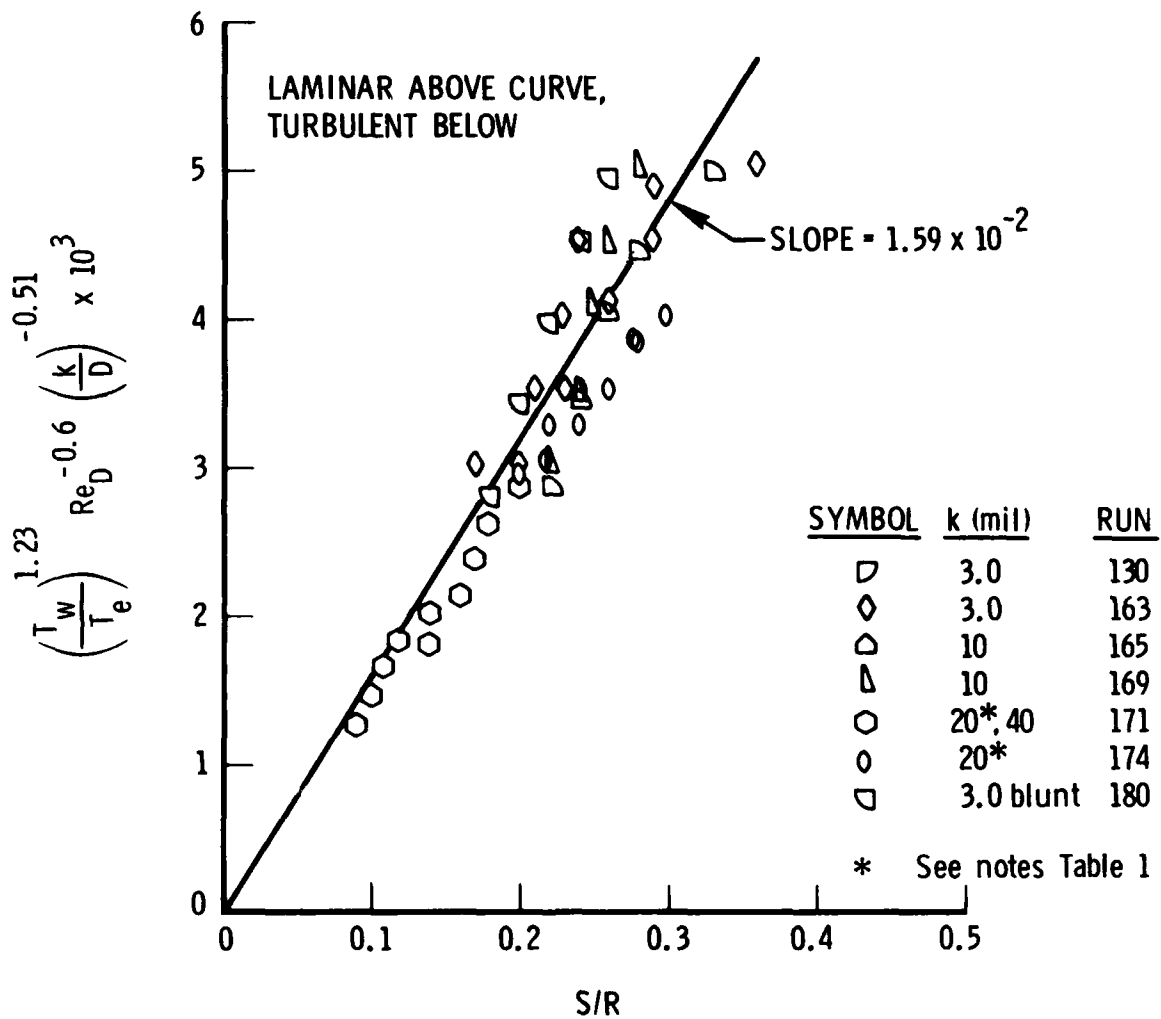


Figure 2. PANT, $M = 5.0$: Correlation of Data in Region of Concave Flow Curvature

points that fall below Eq. (3), is shown in Figure 3. Once again agreement is relatively good. In this case the slope of the straight line has changed to 0.99×10^{-2} , due to the change in M_∞ . Additional data is also available in correlating this Mach number effect. Figure 4 shows various other wind tunnel tests. The Mach number in these tests ranges from 3.0 to 10.4. Once again the data fall on the correlation in Eq. (3) except for those points approaching the stagnation region. The $M = 10.4$ data¹⁰ is especially low. The values of the right side of Eq. (4) have been calculated for these latter points and, together with the slopes for the PANT and ART data from Figures 2 and 3, are plotted versus M_∞ in Figure 5. Because of the abundance of PANT and ART data, the correlation in Figure 5 is drawn through these points. This final correlation for the region of concave flow curvature is given by

$$\frac{k}{D} = 152 \left[\frac{(T_w/T_e)^{1.23}}{S/R} \frac{M_\infty}{Re_D^{0.6}} \right]^{1.96} \quad (5)$$

where k/D is that value of dimensionless roughness required to produce transition. Note the strong dependence on T_w/T_e and M_∞ . Some of the Deveikis and Walker¹¹ data falls slightly below this correlation (Figure 5) as well as below the previous correlation (Figure 4). This data (as well as some of the PANT and ART data) falls in an intermediate zone between the concave and convex flow regions, and does not fall exactly on either correlation. While this error is not great, its significance is that it marks the downstream limit of the concave flow region. For the $M_\infty = 5$ or 8 data, this limit is

¹⁰J. C. Dunavant and H. W. Stone, Effect of Roughness on Heat Transfer to Hemisphere Cylinders at Mach Numbers 10.4 and 11.4, NASA TN D-3871, Langley Research Center, Hampton, Virginia (March 1967).

¹¹W. D. Deveikis and R. W. Walker, Local Aerodynamic Heat Transfer and Boundary-Layer Transition on Roughened Sphere-Ellipsoid Bodies at Mach Number 3.0, NASA TN D-907, Hampton, Virginia (August 1961).

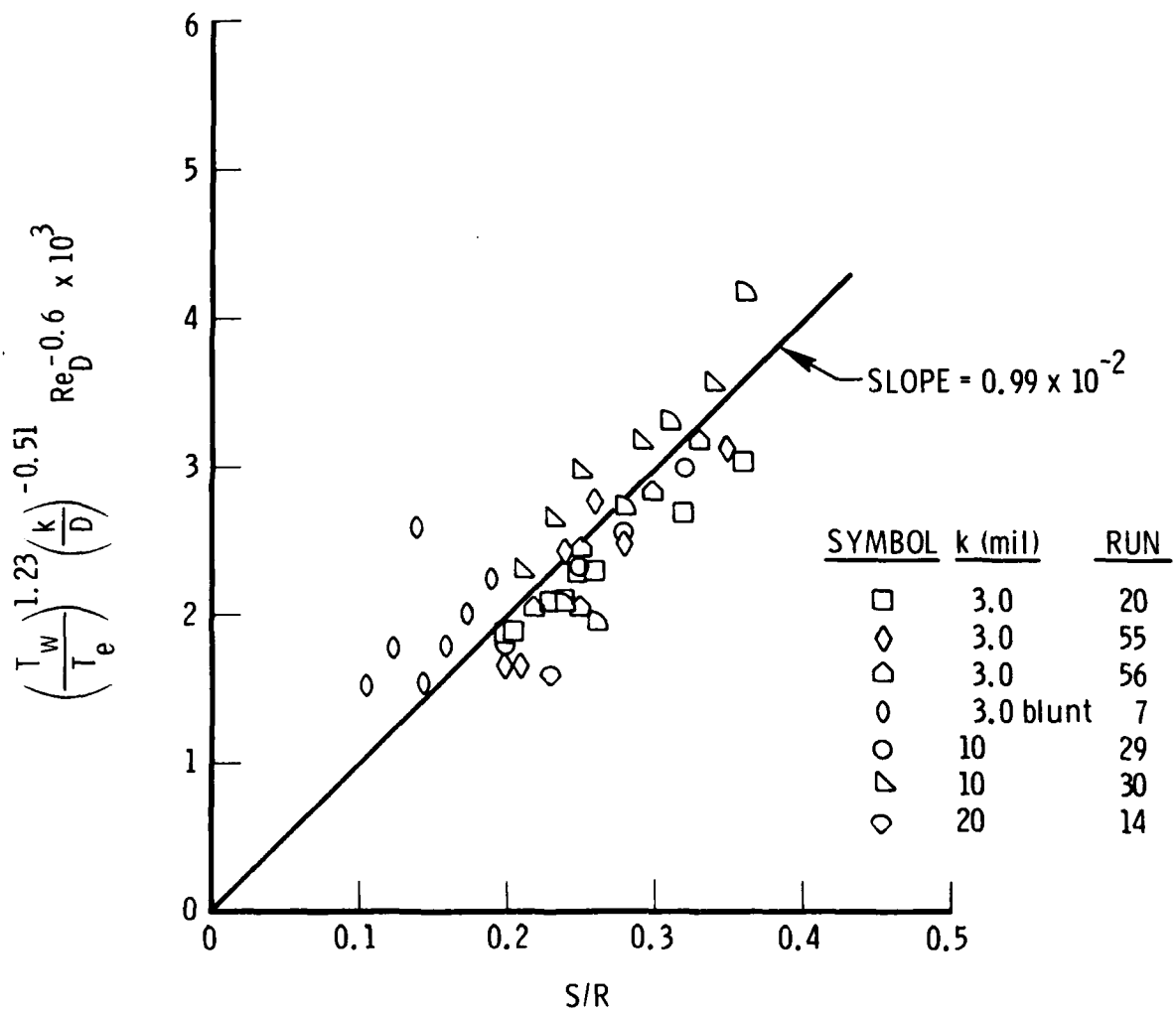


Figure 3. ART, M = 7.9: Correlation of Data in Region of Concave Flow Curvature

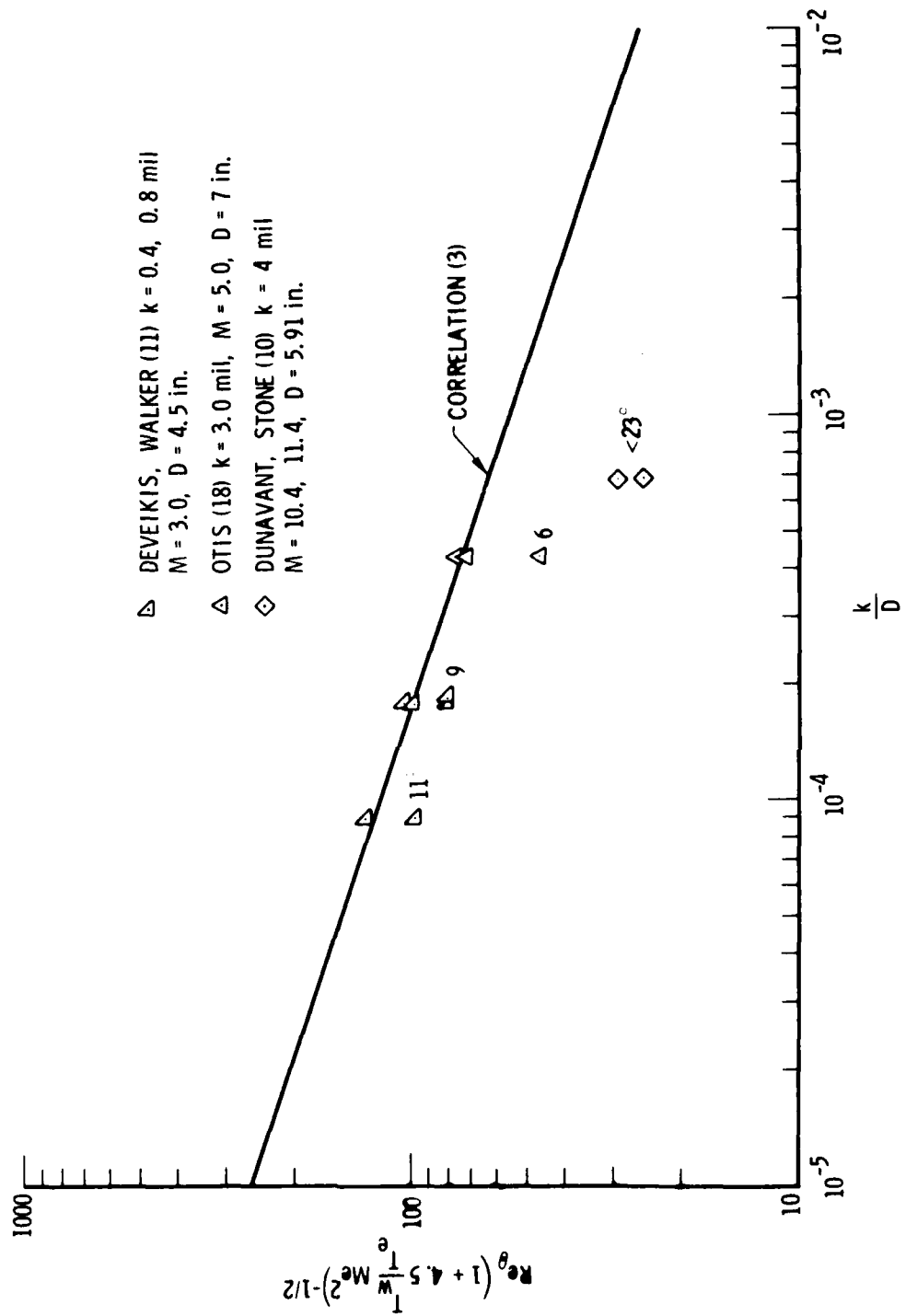


Figure 4. Additional Wind Tunnel Tests

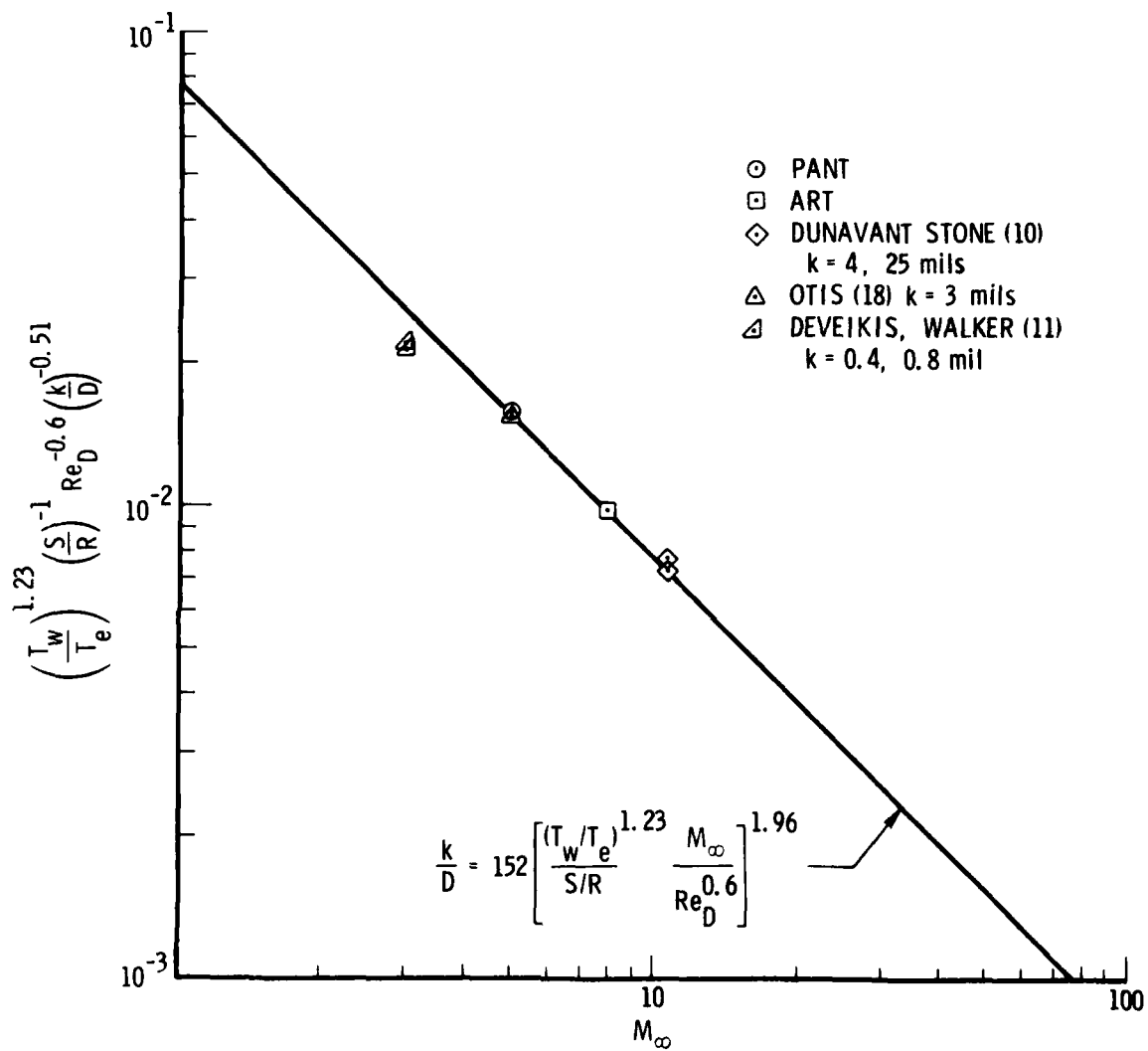


Figure 5. Correlation of Data in Region of Concave Flow Curvature

approximately at $S/R = 0.3$. For the $M_\infty = 10.4$ it extends approximately to $S/R = 0.40$. In general the limit of the concave region will be affected by Re_D through boundary layer development. For increasing M_∞ one expects that the decreasing shock standoff distance will increase the required flow curvature. However increasing M_∞ also lowers the Reynolds number behind the shock, so the effect of M_∞ is not yet clear. Nevertheless, it appears that for relatively high Re_D and M_∞ the concave curvature region may extend over most of the nose. This will be discussed in more detail in Section F.

C. COMPARISON WITH CORRELATION FOR TWO-DIMENSIONAL TRIPS

For the case of a flat plate with a single two-dimensional trip (a wire), Schlichting¹² quotes the following low speed (incompressible) correlation for transition at the trip itself:

$$\frac{k}{\nu} \sqrt{\frac{\tau}{\rho}} = 20 \quad (6)$$

where τ is the wall shear evaluated at the trip position. For a flat plate

$$\tau = 0.332 \mu u_e \sqrt{\frac{u_e}{\nu x}} \quad (7)$$

and

$$Re_\theta = 0.664 \sqrt{\frac{u_e x}{\nu}} \quad (8)$$

¹²H. Schlichting, Boundary-Layer Theory, 6th ed., McGraw-Hill Book Co., New York, p 511 (1968).

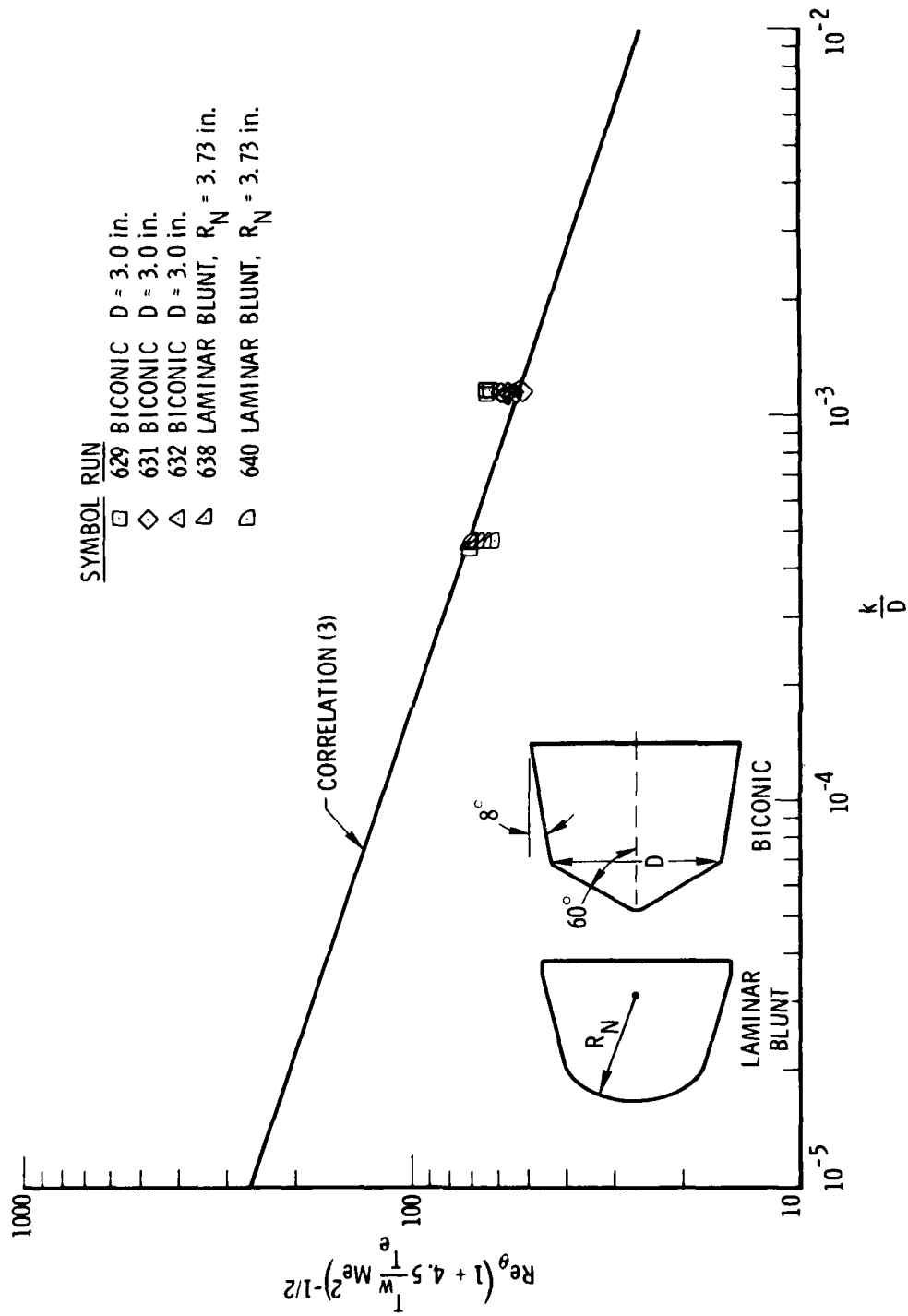
where u_e is the edge velocity and x is the trip distance from the leading edge. Substitution of Eq. (7) and Eq. (8) into Eq. (6) gives

$$Re_{\theta} = 0.96 \left(\frac{k}{x} \right)^{-2/3} \quad (9)$$

Equation (9) has the same form as the zero M_e limit of the correlation in Eq. (3), except that k is nondimensionalized by x rather than D and the power on k is exactly twice that given by Eq. (3). This higher power is attributed to the fact that three-dimensional disturbances may dissipate in all directions (away from the wall), whereas two-dimensional disturbances may not dissipate in the direction parallel to the trip. The correspondence between these two correlations tends to confirm the validity of both of them. It also suggests that wall shear could have been used instead of Re_{θ} in the present correlation.

D. PANT SERIES J DATA²

These data are important because shapes other than the hemisphere or truncated hemisphere are included. The two shapes of interest here are the laminar blunt and the biconic. The former shape is typical of a laminar ablating nosetip; the latter shape sometimes occurs after transition has altered the original nosetip shape. These data are correlated in Figure 6. For these test models, the measured roughness varied from 2.7 to 3.6 mils. A nominal roughness of 3.5 mils was used for the correlation. The data agrees well given the measured variation in roughness. For laminar blunt tests, D was obtained from the actual nose radius. For the biconic tests, the diameter of the body at the shoulder was used as D . It is probably coincidental that this latter data agree so well using this D . The point to be made is that the biconic data can be correlated with Eq. (3) using some appropriate D . Some of the laminar blunt data (not shown on Figure 6) falls within the concave curvature region. This is shown with the appropriate correlation from Eq. (5) in Figure 7. Once again the agreement is good.



SYMBOL	RUN	GEOMETRY	D
□	629	BICONIC	3.0 in.
◇	631	BICONIC	3.0 in.
△	632	BICONIC	3.0 in.
▴	638	LAMINAR BLUNT	$R_N = 3.73$ in.
◻	640	LAMINAR BLUNT	$R_N = 3.73$ in.

Figure 6. PANT Series J

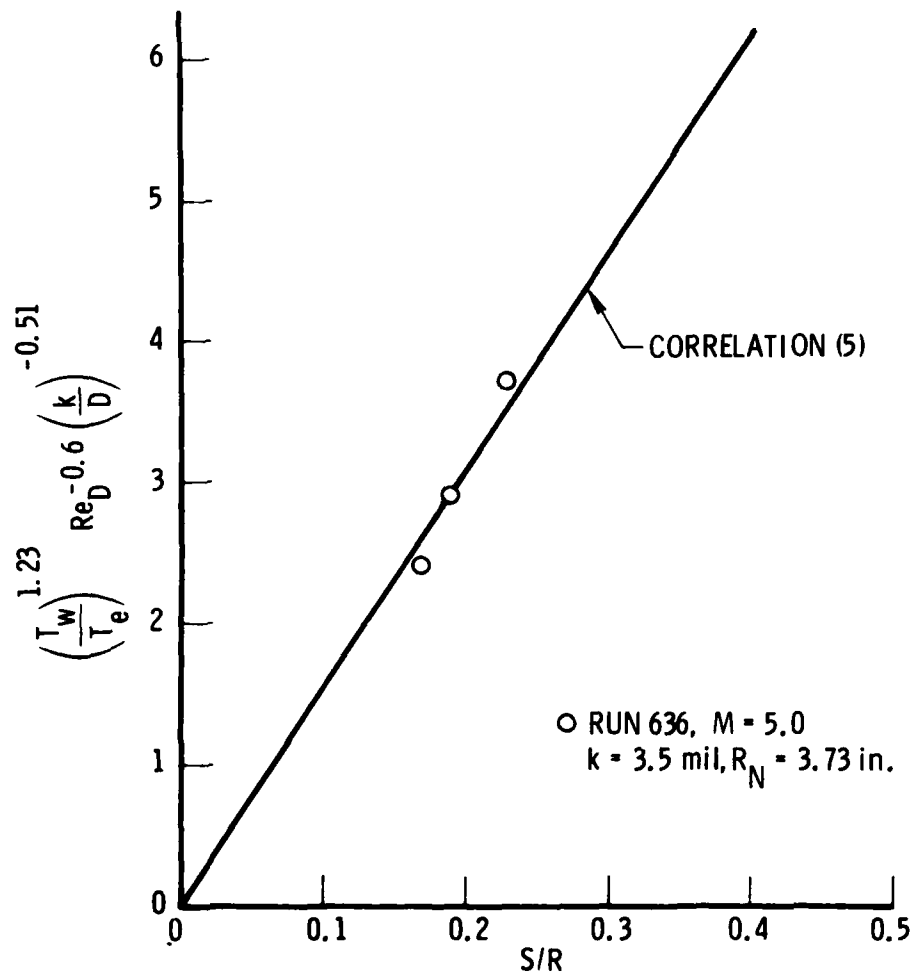


Figure 7. Laminar Blunt - Series J

E. 50-MW ARC DATA

The data presented in Figure 8 consist of seven points previously reduced by Anderson¹. The data are used exactly as given in this reference. The roughnesses used are the k_{85} values discussed earlier. These were obtained from distributions measured by Kratsch, et al¹³ and Swain, et al¹⁴ on postlaminar test specimens of ATJS graphite and MOD 111-A carbon-carbon. With the exception of one anomalous point, the agreement is extremely good. Blowing was not included in the momentum thickness calculation. This would slightly lower Re_{θ} . Two important observations can be made from these data. First, there is no apparent noise influence in the data. This has long been a source of uncertainty in the 50-MW data. Second, there is no apparent "in situ" roughness effect, i.e., the post test roughness used in the correlation appears to be very close to the actual roughness during the test. Obviously many more tests have to be examined, but data of this type could have great value.

Figure 9 is a typical ATJS roughness distribution¹⁵ and is shown in order to demonstrate the selection of the k_{85} value.* The roughness height distribution has a sharp knee at a value of 0.15 (corresponding to k_{85}) on the ordinate. From this point, the spacing between elements increases rapidly as roughness height is increased (this assumes large spacings are associated with large roughness elements) implying that elements larger than this will be less likely to form a continuous transition line (but will tend to produce

*The fact that these larger roughness elements might determine the mean transition front was originally suggested to the author by D. C. Reda of the Naval Surface Weapons Center (NSWC).

¹³K. M. Kratsch, et al., Erosion Mechanisms and Improvement of Graphitic Materials, Vol. II, Hyperthermal Erosion Tests and Surface Roughness Characterization, AFML-TR-70-307, Vol. II, McDonnell Douglas Astronautics Co., Huntington Beach, California (June 1972).

¹⁴C. E. Swain, R. B. Dirling, Jr., and J. D. Baldwin, Erosion Mechanisms and Improvement of Graphitic Materials, AFML-TR-73-286, McDonnell Douglas Astronautics Co., Huntington Beach, California (November 1973).

¹⁵R. B. Dirling, Jr. and K. M. Kratsch, Graphite Microroughness and Material Property Characterization Tests, MDCG5788, McDonnell Douglas Astronautics Co., Huntington Beach, California (April 1975).

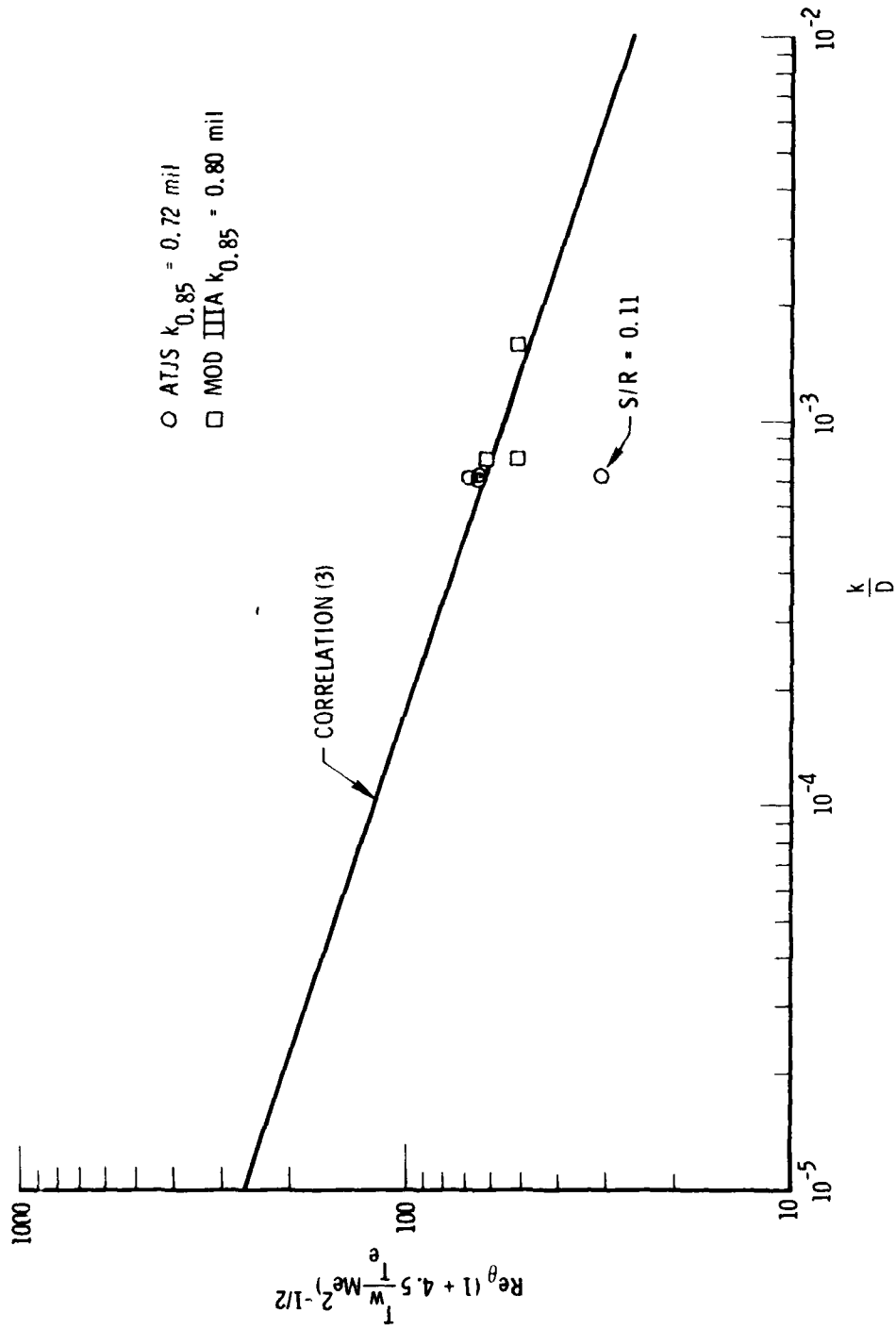


Figure 8. 50-MW Arc Data

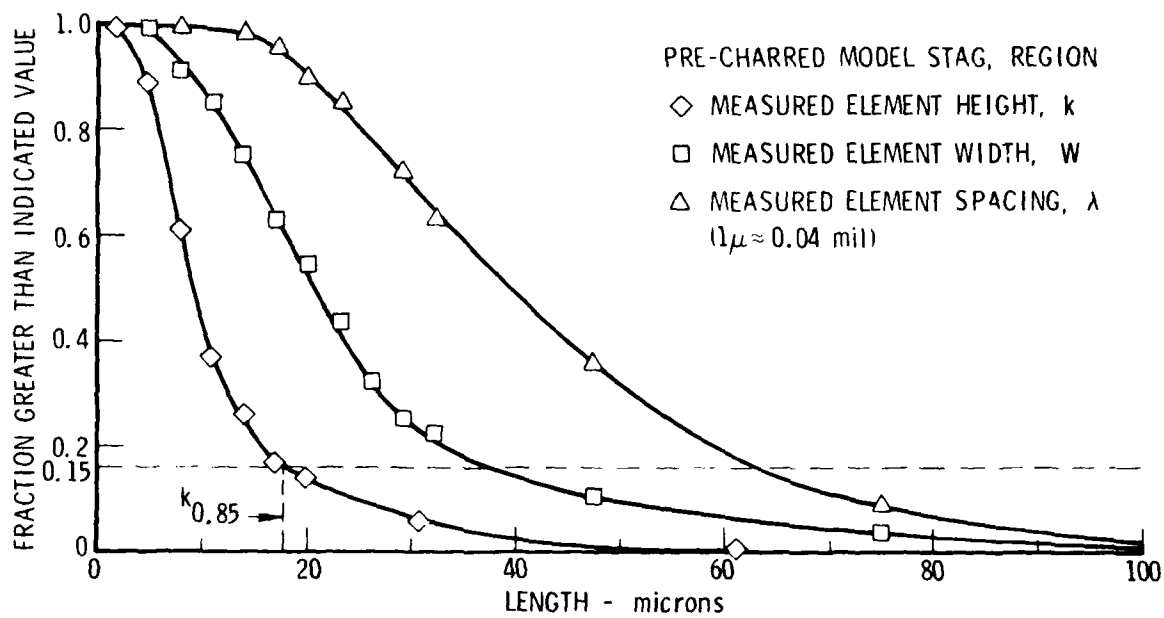


Figure 9. Distribution of Microroughness Characteristics

forward transition points or asymmetries). The k_{85} elements, however, are associated with a width of approximately 40μ and a spacing of approximately 65μ , thus forming a nearly continuous front.

F. DEMETRIADES, LADERMAN DATA¹⁶

These data are taken on a 7-in. nose radius hemisphere at $M = 6.0$ under near-adiabatic wall conditions. Point of transition is determined using both hot wire and pitot tube. The data are compared with the concave curvature correlation from Eq. (5) in Figure 10. The 2.36-mil data roughly straddles the correlation, hot wire above, pitot below. The 4.77-mil data is high. This discrepancy is thought to be due to the fact that the boundary layer temperature distribution for this adiabatic case is radically different from the cold-wall tests used to form the correlation. This could be corrected, but future tests are planned using a cold wall. The data, which will be looked at in toto at that time, are important because the Goertler vortex region appears to extend to about $S/R = 1.0$, possibly because Re_D is higher than most of the previous data (but still lower than low altitude flight), or because of the higher T_w/T_e values. This tends to indicate that for typical flight trajectories most of the nose is in the concave flow region.

¹⁶A. Demetriades and A. J. Laderman, Advanced Penetration Problems Program, SAMSO-TR-75-51, Vols. I and II, Space and Missile Systems Organization, Air Force Systems Command, Los Angeles, California (December 1974).

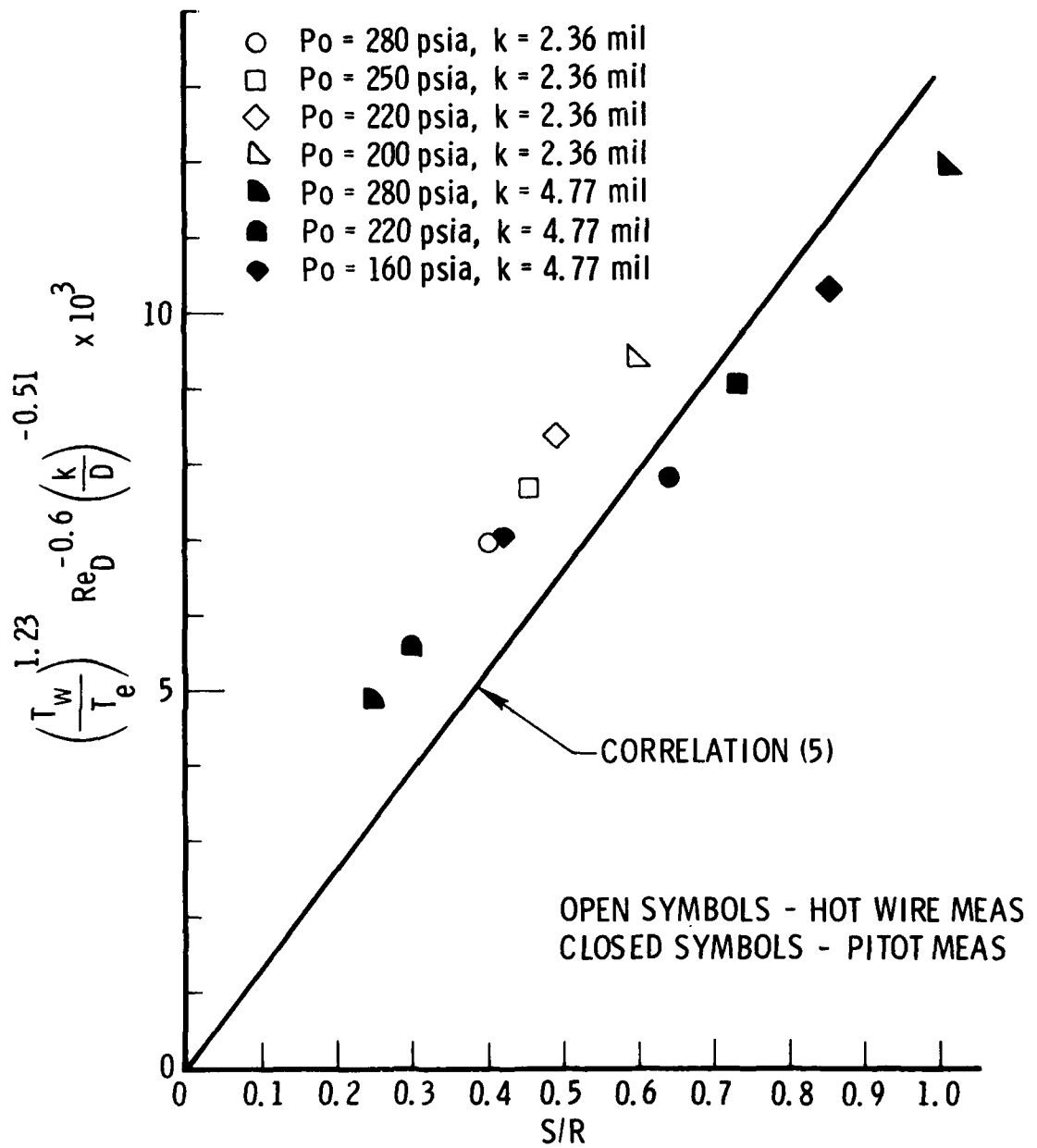


Figure 10. Demetriades, Ladermann Data

III. CONCLUSIONS

The extension of the correlation to very small roughness, i. e., $10 \mu\text{in.}$ in Figure 1b, implies that there are no "smooth" walls. In the absence of noise, some Reynolds number will eventually produce transition no matter how small the roughness. Previous correlations using only a single correlation for both the concave and convex flow regions show a greater k dependence. For instance, PANT uses a power on k of -0.7 rather than the $-1/3$ used here. This made the correlation too high at small roughnesses and led to the necessity of introducing a "smooth wall limit" or freestream noise to explain the observed early onset.

Correspondingly, this correlation shows no apparent influence of freestream noise--either in the wind tunnel or flight tests. Even the 50-MW data show no evidence of noise. One could argue that noise was the dominating factor in these latter tests and the results fell coincidentally on the correlation, but this would require some strong substantiation. Noise can become a factor if experimenters go out of their way to make it so. This is apparently the case for data taken by Dunlap and Keuthe¹⁷ where a sphere was shrouded in an attempt to simulate hypersonic flow. Data for these tests (not presented here) fall far below the present correlations, probably because of interaction between the shroud and the model. Thus, it seems that data scatter previously thought due to noisy test conditions is more likely due to the correlations used. It appears that roughness elements tend to become significant disturbances in high speed flows, while freestream noise may become "smeared out" in the associated large velocity gradients. Alternately, in low speed flows, noise is often dominating. Wind tunnel tests of highly polished models, which were not studied here, are possibly noise influenced.

¹⁷R. Dunlap and A. M. Kuethe, "Effects of Cooling on Boundary-Layer Transition on a Hemisphere in Simulated Hypersonic Flow," Journal of the Aeronautical Sciences, 29, 1454-1462 (December 1962).

Nosetip asymmetry depends on the random distribution of roughness heights and will always be present if significant size variation exists.

Roughness spacing, shape, various statistical characteristics (other than k distribution), etc., appear to have much less influence on transition than the properties correlated here. This applies only to the types of roughnesses studied here; however, a large variation from these types may produce an effect.

IV. RECOMMENDATIONS

The correlation in Eq. (5) for the concave curvature region is strongly sensitive to the power on Mach number and requires a fairly large extrapolation to flight conditions. It is thus desirable that accurate higher M_∞ test data be obtained in order to check the validity of the correlation and its extension around the nosetip. Wind tunnel tests using the PANT models would be ideal, but ballistic range data would also be very useful if transition location can be determined accurately.

Analytical studies should also be of value to determine the extent of the concave curvature region and to establish some sort of correlation for this. Empirical confirmation of the existence of Goertler vortices is also desirable.

Finally an attempt should be made to apply the correlation in Eq. (3) to frustra transition since there is no obvious reason why it should not work there.

REFERENCES

1. A. D. Anderson, Analysis of PANT Series A Rough Wall Calorimeter Data, Aerotherm Report 73-81, Part II, Aerotherm Division/Acurex Corp., Mountain View, California (1973).
2. M. D. Jackson, Interim Report Passive Noretip Technology (PANT) Program, Aerotherm Report 74-100, Vol. XV, Aerotherm Division/Acurex Corp., Mountain View, California (April 1974).
3. R. E. Phinney and F. P. Baltakis, Influence of Roughness on Heat Transfer and Transition; ART Program Data Report, NOLTR 73-231, Naval Ordnance Laboratory, Silver Spring, Maryland (December 1974).
4. J. B. Peterson and E. A. Horton, An Investigation of the Effect of a Highly Favorable Pressure Gradient on Boundary-Layer Transition as Caused by Various Types of Roughnesses on a 10-Foot-Diameter Hemisphere at Subsonic Speeds, NASA Memo 2-8-59L, National Aeronautics and Space Administration, Washington, D. C. (April 1959).
5. A. E. von Doenhoff and E. A. Horton, A Low-Speed Experimental Investigation of the Effect of a Sandpaper Type of Roughness on Boundary-Layer Transition, Technical Note 3858, National Advisory Committee for Aeronautics, Washington, D. C. (October 1956).
6. L. Lees, "Note of the Stabilizing Effect of Centrifugal Forces on the Laminar Boundary Layer Over Convex Surfaces," Journal of the Aeronautical Sciences, 25, 407-408 (June 1958).
7. E. R. van Driest and C. B. Blumer, "Boundary-Layer Transition at Supersonic Speeds--Three-Dimensional Roughness Effects (Spheres)," Journal of the Aerospace Sciences, 29, 909-916 (August 1962).
8. H. Schlichting, Boundary-Layer Theory, 6th ed., McGraw-Hill Book Co., New York, pp 500-508 (1968).
9. H. Görtler, "Dreidimensionale Instabilität der ebenen Staupunktströmung gegenüber wirbelartigen Störungen," Festschrift, Fifty Years of Boundary-Layer Research, Anniversary Volume, eds. H. Görtler and W. Tollmien, Vieweg, Braunschweig, Germany, pp 303-314 (1955).

10. J. C. Dunavant and H. W. Stone, Effect of Roughness on Heat Transfer to Hemisphere Cylinders at Mach Numbers 10.4 and 11.4, NASA TN D-3871, Langley Research Center, Hampton, Virginia (March 1967).
11. W. D. Deveikis and R. W. Walker, Local Aerodynamic Heat Transfer and Boundary-Layer Transition on Roughened Sphere-Ellipsoid Bodies at Mach Number 3.0, NASA TN D-907, Hampton, Virginia (August 1961).
12. H. Schlichting, Boundary-Layer Theory, 6th ed., McGraw-Hill Book Co., New York, p 511 (1968).
13. K. M. Kratsch, et al., Erosion Mechanisms and Improvement of Graphitic Materials, Vol. II, Hyperthermal Erosion Tests and Surface Roughness Characterization, AFML-TR-70-307, Vol. II, McDonnell Douglas Astronautics Co., Huntington Beach, California (June 1972).
14. C. E. Swain, R. B. Dirling, Jr., and J. D. Baldwin, Erosion Mechanisms and Improvement of Graphitic Materials, AFML-TR-73-286, McDonnell Douglas Astronautics Co., Huntington Beach, California (November 1973).
15. R. B. Dirling, Jr. and K. M. Kratsch, Graphite Microroughness and Material Property Characterization Tests, MDCG5788, McDonnell Douglas Astronautics Co., Huntington Beach, California (April 1975).
16. A. Demetriades and A. J. Laderman, Advanced Penetration Problems Program, SAMSO-TR-75-51, Vols. I and II, Space and Missile Systems Organization, Air Force Systems Command, Los Angeles, California (December 1974).
17. R. Dunlap and A. M. Kueth, "Effects of Cooling on Boundary-Layer Transition on a Hemisphere in Simulated Hypersonic Flow," Journal of the Aeronautical Sciences, 29, 1454-1462 (December 1962).
18. J. H. Otis, Jr., et al., Strategic Reentry Technology Program (Street-A) Final Report, AVSD-0210-70-RR, Vol. II, Avco Systems Division, Wilmington, Massachusetts (November 1970).
19. M. R. Wool, Interim Report Passive Noretip Technology (PANT) Program, Aerotherm Report 74-100, Vol. X, Aerotherm Division/Acurex Corp., Mountain View, California (January 1975).

20. J. J. Buglia, Heat Transfer and Boundary-Layer Transition on a Highly Polished Hemisphere-Cone in Free Flight at Mach Numbers up to 3.14 and Reynolds Numbers up to 24×10^6 , NASA TN D-955, Langley Research Center, Hampton, Virginia (September 1961).
21. J. R. Hall, K. C. Speegle, and R. O. Piland, Preliminary Results From a Free-Flight Investigation of Boundary-Layer Transition and Heat Transfer on a Highly Polished 8-Inch-Diameter Hemisphere-Cylinder at Mach Number and Reynolds Numbers Based on Length of 1 Foot up to 17.7×10^6 , NACA RM L57D18c, Langley Aeronautical Laboratory, Langley Field, Virginia (May 1957).
22. B. J. Garland and L. T. Chauvin, Measurements of Heat Transfer and Boundary-Layer Transition on an 8-Inch-Diameter Hemisphere-Cylinder in Free Flight for a Mach Number, NACA RM L57D04a, Langley Aeronautical Laboratory, Langley Field, Virginia (April 1957).
23. C. A. Powars, et al., AFFDL 50 MW RENT Facility Calibration, AFML-TR-73-128, Vol. II, Aerotherm Division/Acurex Corporation, Mountain View, California (October 1973).

NOMENCLATURE

a	speed of sound
D	diameter of nose, nose radius $\times 2$
H	enthalpy
k	average peak to valley (PTV) roughness height
k_{85}	value of k greater than 85% of other roughness element heights
M	Mach number
P	pressure
R	nose radius
Re_D	freestream Reynolds number based on nose diameter (D = 2R)
Re_θ	momentum thickness Reynolds number, $u_e \theta / \nu_e$
S	streamwise distance from the stagnation point
T	temperature
u	streamwise velocity component
U_∞	freestream velocity
θ	momentum thickness (smooth wall)
λ	peak-to-peak spacing between roughness elements
μ	dynamic viscosity; also microns
ν	kinematic viscosity
ρ	density
τ	wall shear at trip location

Subscripts

e boundary-layer edge
w wall
o model stagnation condition
 ∞ freestream

Table 1. Collected Transition Data
(superscript letters refer to notes following table)

PANT SERIES A¹: $M_\infty = 5$, $D = 5.0$ in., HEMISPHERE - 8° cone

Run No.	k (a) (mil)	M_∞	T_o (°R)	Po (atm)	Re_D $\times 10^{-6}$	Ray (deg)	S/R (c)	T_w/T_e	Me	u_e/ν_e $10^6/\text{ft}$	θ (d) ft $\times 10^4$
104	0.6 ^(e)	5.01	1240	2.60	4.21	0	0.33	0.47	0.43	2.54	0.51
						180	0.38	0.58	0.50	2.86	0.50
							0.47	0.68	0.62	3.35	0.51
							0.51	0.76	0.68	3.55	0.51
							0.35	0.47	0.46	2.67	0.52
							0.38	0.58	0.50	2.82	0.50
							0.44	0.67	0.58	3.20	0.50
							0.54	0.77	0.72	3.67	0.51
105	0.6 ^(e)	5.00	1245	2.01	3.22	0	0.40	0.48	0.53	2.30	0.60
						180	0.52	0.59	0.69	2.76	0.61
							0.55	0.68	0.73	2.86	0.61
							0.58	0.75	0.78	2.94	0.61
							0.42	0.48	0.56	2.38	0.60
							0.44	0.58	0.58	2.46	0.59
							0.49	0.66	0.65	2.66	0.59
							0.56	0.74	0.75	2.88	0.60

Table 1. Collected Transition Data (Continued)
 (superscript letters refer to notes following table)

PANT SERIES A¹: $M_\infty = 5$, $D = 5.0$ in., HEMISPHERE - 8° cone

Run No.	$k^{(a)}$ (mil)	M_∞	T_0 (°R)	P_0 (atm)	Re_D $\times 10^{-6}$	$Ray^{(b)}$ (deg)	$S/R^{(c)}$	T_w/T_e	Me	u_e/v_e $10^6/ft$	$\theta^{(d)}$ $ft \times 10^4$
113	1.6 ^(e)	4.99	1240	1.54	2.48	0	0.31	0.47	0.41	1.43	0.66
							0.35	0.57	0.46	1.58	0.65
							0.35	0.65	0.46	1.58	0.63
							0.53	0.75	0.70	2.15	0.67
							0.59	0.82	0.79	2.29	0.68
						180	0.23	0.46	0.30	1.08	0.65
							0.33	0.56	0.43	1.51	0.64
							0.36	0.65	0.48	1.62	0.63
							0.38	0.72	0.50	1.70	0.62
							0.42	0.77	0.56	1.84	0.62
115	1.6 ^(e)	4.98	1210	1.72	1.71	0	0.42	0.48	0.56	1.26	0.83
							0.57	0.58	0.76	1.54	0.88
						180	0.40	0.48	0.53	1.22	0.82
							0.45	0.56	0.60	1.33	0.82
129	3.0 ^(e)	4.98	1220	0.53	0.85	90	0.40	0.45	0.53	0.63	1.16
							0.42	0.49	0.56	0.65	1.15
							0.44	0.54	0.58	0.67	1.15
							0.48	0.58	0.64	0.71	1.16
							0.50	0.62	0.66	0.74	1.15

Table 1. Collected Transition Data (Continued)
 (superscript letters refer to notes following table)

PANT SERIES A¹: $M_\infty = 5$, $D = 5.0$ in., HEMISPHERE - 8° cone

Run No.	$k^{(a)}$ (mil)	M_∞	T_o (°R)	P_o (atm)	Re_D $\times 10^{-6}$	Ray ^(b) (deg)	$S/R^{(c)}$	T_w/T_e	Me	u_e/ν_e $10^6/\text{ft}$	$\theta^{(d)}$ $\text{ft} \times 10^4$
130	3.0	4.98	1250	1.06	1.69	90	0.22	0.44	0.29	0.71	0.80
							0.24	0.51	0.31	0.77	0.78
							0.26	0.58	0.34	0.83	0.76
							0.28	0.63	0.37	0.89	0.75
							0.33	0.69	0.43	1.02	0.75
132	3.0	4.97	1445	0.66	0.85	90	0.38	0.39	0.50	0.61	1.17
							0.38	0.44	0.50	0.61	1.15
							0.42	0.50	0.56	0.66	1.15
							0.46	0.55	0.61	0.71	1.15
							0.49	0.59	0.65	0.74	1.15
162	3.0 ^(f)	4.97	1200	0.53	0.88	90	0.43	0.48	0.57	0.66	1.17
							0.52	0.53	0.69	0.75	1.20
						180	0.48	0.49	0.64	0.71	1.20
163	3.0	4.98	1200	1.05	1.76	90	0.20	0.47	0.25	0.66	0.77
							0.23	0.53	0.30	0.76	0.76
							0.26	0.60	0.34	0.85	0.74
							0.29	0.65	0.38	0.95	0.73
							0.36	0.71	0.48	1.14	0.74

Table 1. Collected Transition Data (Continued)
 (superscript letters refer to notes following table)

PANT SERIES A¹: $M_\infty = 5$, $D = 5.0$ in., HEMISPHERE - 8° cone

Run No.	k ^(a) (mil)	M_∞	T_o (°R)	P_o (atm)	Re_D $\times 10^{-6}$	Ray ^(b) (deg)	S/R ^(c)	T_w/T_e	Me	u_e/ν_e $10^6/\text{ft}$	θ ^(d) $\text{ft} \times 10^4$
163	3.0	4.98	1200	1.05	1.76	180	0.17	0.47	0.22	0.57	0.77
							0.21	0.53	0.27	0.70	0.75
							0.22	0.59	0.29	0.73	0.74
							0.24	0.65	0.31	0.79	0.73
							0.29	0.69	0.38	0.95	0.72
165	10.0 ^(f)	4.96	1200	0.21	0.35	0	0.31	0.46	0.40	0.203	1.75
							0.31	0.49	0.40	0.203	1.74
							0.68	0.58	0.92	0.345	2.08
						90	0.30	0.46	0.39	0.198	1.75
							0.31	0.49	0.41	0.203	1.74
							0.54	0.55	0.72	0.309	1.91
169	10.0	4.97	1200	0.39	0.64	0	0.20	0.46	0.25	0.250	1.26
							0.22	0.50	0.29	0.273	1.24
							0.23	0.54	0.30	0.285	1.23
							0.24	0.58	0.31	0.297	1.22
							0.26	0.61	0.34	0.320	1.20

Table 1. Collected Transition Data (Continued)
 (superscript letters refer to notes following table)

PANT SERIES A¹; $M_\infty = 5$, $D = 5.0$ in., HEMISPHERE - 8° cone

Run No.	$k^{(a)}$ (mil)	M_∞	T_o (°R)	P_o (atm)	$Re_D \times 10^{-6}$	Ray ^(b) (deg)	$S/R^{(c)}$	T_w/T_e	Me	$u_e/\sqrt{v_e}$ $10^6/ft$	$\theta^{(d)}$ $ft \times 10^4$
169	10.0	4.97	1200	0.39	0.64	90	0.22	0.29	0.46	0.273	1.26
							0.24	0.31	0.50	0.297	1.25
							0.25	0.33	0.54	0.308	1.23
							0.26	0.34	0.58	0.320	1.22
							0.28	0.37	0.61	0.343	1.21
171	20.0 ^(g)	4.97	1215	0.52	0.86	0	0.14	0.47	0.19	0.232	1.10
							0.16	0.54	0.21	0.264	1.08
							0.17	0.59	0.22	0.280	1.05
							0.18	0.64	0.23	0.297	1.04
							0.20	0.69	0.25	0.329	1.02
40.0		4.97	1215	0.52	0.86	180	0.09	0.47	0.12	0.149	1.10
							0.10	0.53	0.13	0.166	1.07
							0.11	0.59	0.14	0.183	1.05
							0.12	0.64	0.16	0.199	1.03
							0.14	0.69	0.19	0.232	1.01

Table 1. Collected Transition Data (Continued)
 (superscript letters refer to notes following table)

PANT SERIES A¹: $M_\infty = 5$, $D = 5.0$ in., HEMISPHERE - 8° cone

Run No.	$k^{(a)}$ (mil)	M_∞	T_o (°R)	P_o (atm)	$Re D \times 10^{-6}$	Ray (deg)	$S/R^{(c)}$	T_w/T_e	Me	$u_e/\sqrt{v_e}$ $10^6/\text{ft}$	$\theta^{(d)}$ $\text{ft} \times 10^4$
174	20.0 ^(g)	4.96	1190	0.21	0.354	0	0.22	0.47	0.29	0.147	1.72
							0.24	0.50	0.31	0.160	1.71
							0.26	0.53	0.34	0.173	1.70
							0.28	0.57	0.37	0.185	1.68
							0.30	0.59	0.39	0.198	1.67
							0.20	0.46	0.25	0.135	1.72
							0.22	0.50	0.29	0.147	1.70
							0.24	0.53	0.31	0.160	1.69
							0.28	0.57	0.37	0.185	1.68
							0.30	0.59	0.39	0.198	1.67

PANT BLUNT^(h) SPHERE-CONE, $D = 10.0$ in.

180	3.0 ^(e)	4.98	1200	1.03	3.43	180	0.18	0.46	0.25	0.64	1.05
							0.20	0.54	0.27	0.70	1.03
							0.22	0.61	0.30	0.77	1.01
							0.24	0.68	0.33	0.84	0.99
							0.26	0.73	0.36	0.90	0.98
181	3.0	4.97	1200	0.52	1.73	180	0.34	0.47	0.48	0.58	1.47
							0.36	0.50	0.51	0.61	1.45

Table 1. Collected Transition Data (Continued)
 (superscript letters refer to notes following table)

PANT SERIES J²: M_∞ = 5, BICONIC⁽ⁱ⁾, D = 3.0 in., R = 0.25 in.

Run No.	k ^(a) (mil)	M _∞	To (°R)	Po (atm)	Re D × 10 ⁻⁶	Ray ^(b) (deg)	S/R ^(c)	T _w /T _e	Me	u _e /v _e 10 ⁶ /ft	θ ^(d) ft × 10 ⁴
629	3.5 ^(e)	4.97	1310	0.60	0.53	-	3.07	0.45	0.44	0.57	1.33
							3.60	0.54	0.45	0.58	1.36
							3.89	0.63	0.46	0.59	1.35
631	3.5	4.97	1300	0.43	0.39	-	4.99	0.46	0.51	0.46	1.59
							5.16	0.54	0.51	0.47	1.53
							5.39	0.61	0.62	0.51	1.43
632	3.5	4.98	1310	0.72	7.62	-	1.97	0.47	0.41	0.65	1.04
							2.15	0.58	0.41	0.65	1.03
							2.44	0.67	0.42	0.66	1.03

PANT SERIES J: LAMINAR ABLATED^(j), D = 2R = 7.46 in.

636	3.5 ^(e)	4.99	1330	1.16	2.54	-	0.17	0.42	0.23	0.58	0.93
							0.19	0.49	0.25	0.65	0.92
							0.23	0.60	0.31	0.78	0.88
638	3.5	4.97	1300	0.58	1.29	-	0.33	0.43	0.45	0.56	1.35
							0.43	0.53	0.60	0.70	1.35
							0.56	0.66	0.82	0.83	1.39

Table 1. Collected Transition Data (Continued)
 (superscript letters refer to notes following table)

PANT SERIES J²: LAMINAR ABLATED^(j), D = 2R = 7.46 in.

Run No.	k ^(a) (mil)	M _∞	To (°R)	Po (atm)	Re D × 10 ⁻⁶	Ray ^(b) (deg)	S/R ^(c)	T _w /T _e	Me	u _e /v _e 10 ⁶ /ft	θ ^(d) ft × 10 ⁴
640	3.5	4.98	1295	0.69	1.47	-	0.27	0.43	0.36	0.56	1.21
							0.36	0.54	0.49	0.72	1.20
							0.47	0.66	0.67	0.89	1.20

NOL-ART DATA³: M_∞ = 5, BLUNT^(h) SPHERE-CONE, D = 10.0 in.

3	3.0 ^(e)	5.00	1995	1.72	6.09	0	0.10	0.456	0.133	0.597	0.837
						90	0.115	0.557	0.156	0.685	0.807
							0.09	0.456	0.122	0.537	0.837
							0.10	0.507	0.130	0.582	0.821
							0.115	0.557	0.156	0.685	0.807
							0.125	0.646	0.170	0.744	0.781
							0.13	0.683	0.176	0.773	0.700
4	3.0	4.98	1169	1.18	3.99	0	0.15	0.472	0.204	0.773	0.999
						90	0.17	0.473	0.230	0.703	1.000
							0.175	0.549	0.237	0.723	0.972
							0.19	0.652	0.257	0.783	0.936

Table 1. Collected Transition Data (Continued)
 (superscript letters refer to notes following table)

NOL-ART DATA: $M_\infty = 5$, BLUNT^(h) SPHERE-CONE, $D = 10.0$

Run No.	$k^{(a)}$ (mil)	M_∞	T_o (°R)	P_o (atm)	Re_D $\times 10^{-6}$	Ray ^(b) (deg)	$S/R^{(c)}$	T_w/T_e	Me	u_e/v_e $10^6/ft$	$\theta^{(d)}$ $ft \times 10^4$
5	3.0	4.97	1158	0.705	2.63	0	0.25	0.466	0.345	0.627	1.287
							0.26	0.499	0.364	0.654	1.280
							0.27	0.529	0.372	0.667	1.269
							0.275	0.585	0.381	0.682	1.247
							0.28	0.611	0.388	0.692	1.238
						90	0.25	0.466	0.345	0.627	1.287
							0.265	0.499	0.364	0.654	1.280
							0.28	0.610	0.385	0.687	1.237

NOL-ART: $M = 8$, BLUNT^(h)

7	3.0 ^(e)	7.90	1432	1.21	7.08	0	0.105	0.398	0.141	0.357	1.143
							0.125	0.451	0.170	0.423	1.123
							0.14	0.612	0.189	0.474	1.059
						90	0.145	0.400	0.195	0.490	1.146
							0.16	0.452	0.216	0.540	1.126
							0.175	0.499	0.237	0.588	1.108
							0.19	0.543	0.257	0.638	1.092
8	3.0	7.91	1423	0.991	5.89	0	0.16	0.389	0.212	0.439	1.267
							0.17	0.435	0.230	0.472	1.247

Table 1. Collected Transition Data (Continued)
 (superscript letters refer to notes following table)

NOL-ART: M = 8, BLUNT^(h)

Run No.	k ^(a) (mil)	M _∞	To (°R)	Po (atm)	Re _D × 10 ⁻⁶	Ray ^(b) (deg)	S/R ^(c)	T _w /T _e	Me	u _e /v _e 10 ⁶ /ft	θ ^(d) ft × 10 ⁴
8	3.0	7.91	1423	0.991	5.89	90	0.20	0.391	0.266	0.547	1.270
							0.21	0.437	0.285	0.582	1.249
							0.23	0.479	0.313	0.631	1.229
							0.235	0.518	0.324	0.652	1.212
9	3.0	7.90	1402	0.737	4.47	0	0.28	0.395	0.390	0.582	1.477
							0.305	0.621	0.427	0.630	1.371
						90	0.27	0.394	0.378	0.566	1.471
							0.29	0.416	0.399	0.594	1.470
10	3.0	7.84	1385	0.492	3.00	0	0.03	0.399	0.415	0.417	1.806

NOL-ART: M = 8, HEMISPHERE - 8° cone, D = 5.0 in.

14	20.0 ^(g)	7.79	1348	0.254	0.80	0	0.23	0.410	0.306	0.163	1.72
							0.34	0.455	0.449	0.232	1.74
							0.38	0.554	0.499	0.255	1.71
			180				0.28	0.414	0.371	0.196	1.73
							0.30	0.451	0.395	0.210	1.71
							0.35	0.550	0.462	0.238	1.69

Table 1. Collected Transition Data (Continued)
 (superscript letters refer to notes following table)

NOL-ART: M = 8, HEMISPHERE - 8° cone, D = 5.0 in.

Run No.	k ^(a) (mil)	M _∞	T ₀ (°R)	P ₀ (atm)	Re _D × 10 ⁻⁶	Ray ^(b) (deg)	S/R ^(c)	T _w /T _e	Me	u _e ^{1/2} 10 ⁶ /ft	θ ^(d) ft × 10 ⁴
20	3.0 ^(f)	7.91	1437	0.974	2.85	0	0.20	0.404	0.260	0.508	0.910
							0.24	0.439	0.320	0.603	0.905
							0.26	0.472	0.346	0.651	0.898
							0.40	0.642	0.523	0.949	0.887
							0.46	0.725	0.607	1.052	0.889
						180	0.20	0.404	0.260	0.508	0.910
							0.23	0.439	0.306	0.579	0.904
							0.25	0.471	0.333	0.627	0.896
							0.32	0.536	0.423	0.786	0.891
							0.36	0.593	0.474	0.868	0.888
							0.40	0.642	0.523	0.949	0.887
							0.46	0.725	0.607	1.052	0.889
21	3.0	7.90	1421	0.737	2.19	0	0.35	0.401	0.462	0.650	1.080
							0.38	0.432	0.499	0.696	1.082
							0.395	0.460	0.517	0.720	1.078
							0.47	0.561	0.621	0.819	1.082
							0.545	0.615	0.728	0.896	1.112

Table 1. Collected Transition Data (Continued)
 (superscript letters refer to notes following table)

NOL-ART: M = 8, HEMISPHERE - 8° cone, D = 5.0 in.

Run No.	k ^(a) (mil)	M _∞	T ₀ (°R)	P ₀ (atm)	Re _D × 10 ⁻⁶	Ray ^(b) (deg)	S/R ^(c)	T _w /T _e	Me	u _e /v _e 10 ⁶ /ft	θ ^(d) ft × 10 ⁴
21	3.0	7.90	1421	0.737	2.19	180	0.32	0.399	0.603	0.603	1.068
							0.345	0.428	0.642	0.642	1.068
							0.365	0.457	0.673	0.673	1.066
							0.38	0.505	0.696	0.696	1.055
							0.425	0.553	0.760	0.760	1.060
							0.525	0.674	0.880	0.880	1.075
22	3.0 ^(f)	7.85	1421	0.535	1.57	0	0.43	0.402	0.566	0.556	1.314
							0.50	0.438	0.661	0.623	1.346
							0.59	0.477	0.795	0.678	1.407
						180	0.425	0.402	0.559	0.552	1.311
							0.48	0.435	0.634	0.604	1.334
29	10.0 ^(f)	7.81	1396	0.296	1.02	0	0.20	0.388	0.260	0.160	1.63
							0.25	0.475	0.333	0.197	1.59
							0.28	0.515	0.371	0.220	1.58
							0.32	0.582	0.423	0.247	1.56
						180	0.30	0.395	0.395	0.235	1.66
							0.33	0.483	0.436	0.254	1.62
							0.37	0.524	0.487	0.279	1.63
							0.41	0.594	0.537	0.304	1.62

Table 1. Collected Transition Data (Continued)
 (superscript letters refer to notes following table)

NOL-ART: M = 8, HEMISPHERE - 8° cone, D = 5.0 in.

Run No.	k ^(a) (mil)	M _∞	T ₀ (°R)	P ₀ (atm)	Re _D × 10 ⁻⁶	Ray ^(b) (deg)	S/R ^(c)	T _w /T _e	Me	u _e /v _e 10 ⁶ /ft	θ ^(d) ft × 10 ⁴
30	10.0	7.79	1375	0.244	0.742	0	0.42	0.421	0.552	0.259	1.884
							0.45	0.476	0.594	0.272	1.879
							0.46	0.522	0.607	0.277	1.859
							0.48	0.552	0.634	0.286	1.859
							0.50	0.603	0.665	0.296	1.850
						180	0.21	0.403	0.276	0.140	1.773
							0.23	0.453	0.306	0.153	1.748
							0.25	0.497	0.333	0.165	1.727
							0.29	0.526	0.383	0.190	1.721
							0.34	0.577	0.449	0.218	1.722
47	1.6 ^(e)	7.90	1492	1.34	3.67	0	0.36	0.393	0.474	1.146	0.831
						180	0.24	0.384	0.320	0.796	0.805
							0.26	0.364	0.346	0.859	0.813
							0.28	0.476	0.371	0.922	0.785
							0.31	0.553	0.409	1.012	0.769
							0.36	0.672	0.474	1.146	0.752

Table 1. Collected Transition Data (Continued)
 (superscript letters refer to notes following table)

NOL-ART: M = 8, HEMISPHERE - 8° cone, D = 5.0 in.

Run No.	k ^(a) (mil)	M _∞	T ₀ (°R)	P ₀ (atm)	Re D × 10 ⁻⁶	Ray ^(b) (deg)	S/R ^(c)	T _w /T _e	Me	$\frac{u_e/\nu_e}{10^6/\text{ft}}$	$\theta^{(d)}$ ft × 10 ⁴
49	1.6	7.90	1461	1.16	3.27	0	0.45	0.407	0.594	1.209	0.916
						180	0.48	0.455	0.634	1.268	0.915
							0.51	0.501	0.676	1.321	0.917
						180	0.40	0.401	0.523	1.109	0.894
							0.45	0.458	0.594	1.208	0.900
							0.475	0.495	0.627	1.259	0.901
55	3.0 ^(e)	7.90	1458	1.04	3.25	0	0.20	0.385	0.260	0.534	0.894
							0.24	0.530	0.320	0.634	0.855
							0.26	0.588	0.346	0.684	0.840
							0.35	0.646	0.462	0.890	0.846
						180	0.21	0.386	0.276	0.559	0.896
							0.28	0.533	0.371	0.734	0.861
							0.35	0.599	0.462	0.890	0.861
							0.40	0.654	0.523	0.997	0.862

Table 1. Collected Transition Data (Continued)
 (superscript letters refer to notes following table)

NOL-ART: M = 8, HEMISPHERE - 8° cone, D = 5.0 in.

Run No.	k ^(a) (mil)	M _∞	T ₀ (°R)	P ₀ (atm)	Re D × 10 ⁻⁶	Ray ^(b) (deg)	S/R ^(c)	T _w /T _e	Me	u _e /v _e 10 ⁶ /ft	θ ^(d) ft × 10 ⁴
56	3.0	7.90	1446	0.799	2.29	0	0.22	0.386	0.291	0.452	1.019
							0.25	0.447	0.333	0.511	1.002
							0.30	0.504	0.395	0.607	0.991
							0.33	0.554	0.436	0.657	0.986
							0.38	0.603	0.499	0.740	0.989
							0.47	0.672	0.621	0.870	1.011
							0.50	0.736	0.661	0.911	1.004
					180		0.25	0.388	0.333	0.510	1.024
							0.35	0.510	0.460	0.690	1.010
							0.38	0.560	0.499	0.740	1.004
							0.40	0.605	0.523	0.773	0.996
57	3.0	7.90	1436	0.675	1.97	0	0.30	0.390	0.395	0.517	1.118
							0.32	0.444	0.423	0.546	1.106
							0.35	0.516	0.462	0.588	1.092
					180		0.38	0.397	0.499	0.630	1.152
							0.40	0.452	0.523	0.658	1.139
							0.41	0.523	0.537	0.670	1.117
							0.425	0.566	0.559	0.688	1.109

Table 1. Collected Transition Data (Continued)
 (superscript letters refer to notes following table)

NOL-ART: M = 8, HEMISPHERE - 8° cone, D = 5.0 in.

Rur No.	k ^(a) (mil)	M _∞	T ₀ (°R)	P ₀ (atm)	Re _D × 10 ⁻⁶	Ray ^(b) (deg)	S/R ^(c)	T _w /T _e	Me	u _e ^{/ve} 10 ⁶ /ft	θ ^(d) ft × 10 ⁴
58	3.0	7.86	1422	0.643	1.68	0	0.42	0.402	0.552	0.657	1.191
							0.45	0.435	0.594	0.691	1.198
							0.48	0.464	0.634	0.726	1.205
							0.53	0.535	0.706	0.770	1.212
							0.43	0.406	0.566	0.668	1.197
							0.47	0.438	0.621	0.714	1.209
							0.49	0.465	0.648	0.737	1.211
							0.53	0.535	0.706	0.770	1.212
60	3.0	7.90	1442	0.800	2.31	0	0.33	0.488	0.436	0.660	1.007
							0.34	0.513	0.449	0.677	1.002
							0.35	0.537	0.462	0.693	0.998
							0.37	0.580	0.487	0.727	0.990
							0.38	0.620	0.499	0.743	0.980
							0.39	0.655	0.511	0.760	0.972
						180	0.29	0.484	0.383	0.591	0.994
							0.32	0.511	0.423	0.644	0.995
							0.34	0.535	0.449	0.677	0.994
							0.35	0.578	0.462	0.693	0.983
							0.37	0.618	0.487	0.727	0.977
							0.40	0.656	0.523	0.777	0.975

Table 1. Collected Transition Data (Continued)
 (superscript letters refer to notes following table)

ADDITIONAL WIND TUNNEL TESTS

DUNAVANT, STONE¹⁰: M ≈ 10, HEMISPHERE-CYLINDER, D = 5.91 in.

Model No.	k ^(k) (mil)	M _∞	T ₀	P ₀ ^(l) (atm)	Re _D × 10 ⁻⁶	S/R	T _w /T _e (m)	Me	u _e /v _e 10 ⁶ /ft	θ ^(l) ft × 10 ⁴
V	4	10.4	1760	0.25	1.12	0.28	0.31	0.31	0.112	2.40
V	4	10.4	1760	0.22	0.98	0.32	0.31	0.38	0.122	2.60

DEVEIKIS, WALKER¹¹: M = 3.0, SPHERE-ELLIPSOID, D = 4.5 in.

1	0.8 ^(e)	3.0	1110	4.51	4.25	0.16	0.49	0.20	2.47 ^(l)	0.333 ^(l)
						0.32	0.95 ⁽ⁿ⁾	0.41	4.80 ^(l)	0.283 ^(l)
2	0.8	3.0	1110	2.95	2.76	0.20	0.49	0.25	2.02 ^(l)	0.417 ^(l)
						0.50	0.95 ⁽ⁿ⁾	0.64	4.22 ^(l)	0.383 ^(l)
3	0.4 ^(e)	3.0	1110	4.51	4.25	0.20	0.44	0.25	3.08 ^(l)	0.333 ^(l)
						0.40	0.95 ⁽ⁿ⁾	0.52	5.87 ^(l)	0.292 ^(l)

OTIS, et al.,¹⁸: M = 5.0, HEMISPHERE, D = 7.0 in.

5	3.0 ^(o)	4.95	1480	3.12	5.14	0.10 ^(l)	0.41 ^(l)	0.13	0.80 ^(l)	0.592 ^(l)
6	3.0	4.96	1499	1.57	2.53	0.25 ^(l)	0.40 ^(l)	0.32	0.97 ^(l)	0.858 ^(l)
7	3.0	4.95	1514	0.63	1.00	0.40 ^(l)	0.39 ^(l)	0.52	0.59 ^(l)	1.46 ^(l)

Table 1. Collected Transition Data (Continued)
(superscript letters refer to notes following table)

DEMETRIADES, LADERMAN¹⁶: $M = 6.0$, HEMISPHERE - 5° cone, $D = 14$ in.

k (mil)	M_∞	T_o (°R)	P_o (atm)	Re_D $\times 10^{-6}$	S/R		T_w/T_e	
					Hot Wire	Pitot	Hot Wire	Pitot
2.36	6.0	850	8.30	6.10	0.40	0.64	1.00	1.10
			7.41	5.48	0.45	0.73	1.03	1.18
			6.52	4.82	0.49	0.86	1.04	1.23
			5.93	4.38	0.59	1.01	1.09	1.32
4.77	6.0	850	8.30	6.10	0.24(p)			1.0
			6.52	4.82	0.30			1.0
			4.74	3.51	0.42			1.03

FLIGHT TEST DATA (Rocket-propelled free-flight)

BUGLIA²⁰: $M_\infty \approx 3$, HEMISPHERE - 14.5° cone, $D = 13.0$ in.

Flight Time (sec)	$k^{(q)}$ (mil)	M_∞	T_o (°R)	P_o (atm)	Re_D $\times 10^{-6}$	S/R	T_w/T_e	Me	$Re_\theta^{(\tau)}$
7.8	0.012	2.97	497	0.70	17.2	0.64	0.62	0.75	798
8.0	0.012	3.14	495	0.68	17.9	0.62	0.58	0.79	804

HALL, SPEEGLE AND PILAND²¹: $M_\infty = 2$ to 3, HEMISPHERE-CYLINDER, $D = 8.0$ in.

2.5	0.020	2.14	525	0.945	9.13	1.29	0.90	1.37	1110
3.0	0.020	2.73	517	0.875	11.3	1.29	0.75	1.46	1200

Table 1. Collected Transition Data (Continued)
 (superscript letters refer to notes following table)

HALL, SPEEGLE AND PILAND²¹: $M_\infty = 2$ to 3, HEMISPHERE-CYLINDER, $D = 8.0$ in.

Flight Time (sec)	$k^{(q)}$ (mil)	M_∞	T_o ($^{\circ}$ R)	P_o (atm)	$Re_D \times 10^{-6}$	S/R	T_w/T_e	Me	Re_θ
3.5	0.020	2.96	513	0.832	11.8	0.94	0.75	1.24	940

GARLAND, CHAUVIN²²: $M_\infty = 2$ to 4, HEMISPHERE-CYLINDER, $D = 8.0$ in.

3.20	0.10	2.50	483	0.892	11.1	0.26	0.54	0.31	235
4.62	0.10	2.80	480	0.762	11.3	0.52	0.89	0.69	435

50-MW ARC DATA (Ref. 1): $M = 1.8$, HEMISPHERE-CYLINDER

Run	Material	k_{85} (mil)	D (in.)	Ho (btu/lbm)	P_o (atm)	S/R	T_w/T_e	$Me^{(u)}$	$Re_\theta^{(v)}$
3-1	ATJS	0.72	1.0	2730	99	0.26	0.88	0.34	83.4
7-2	ATJS	0.72	1.0	5120	83	0.31	0.68	0.40	79.5
9-1	ATJS	0.72	1.0	2240	83	0.11	0.95	0.19	34.0
10-1	ATJS	0.72	1.0	5410	100	0.37	0.66	0.51	87.5
6-1	MOD III-A	0.80	0.5	4160	62	0.70	0.79	0.85	98.6
6-2	MOD III-A	0.80	1.0	4160	62	0.26	0.75	0.34	61.5
8-1	MOD III-A	0.80	1.0	5720	101	0.26	0.65	0.35	73.7

NOTES ON TABLE 1

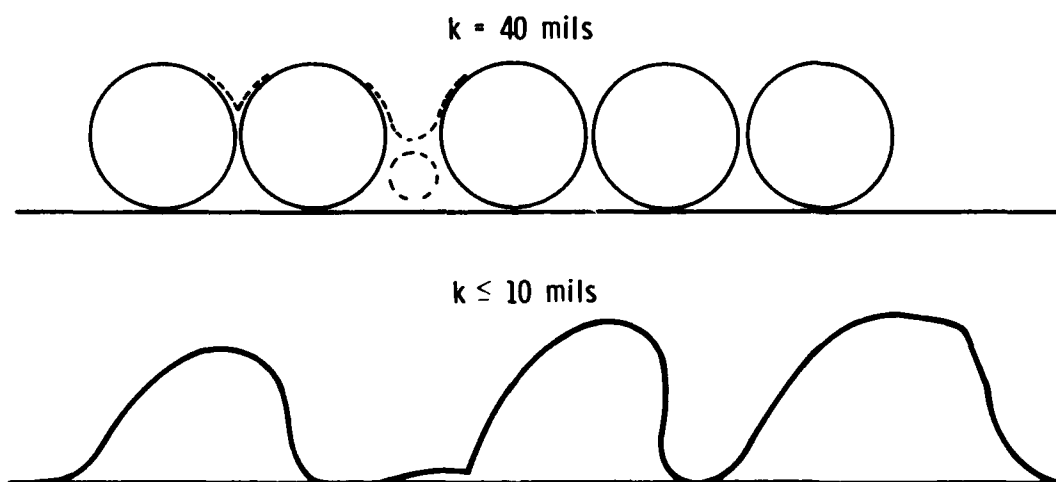
General

For the sake of brevity, detailed discussion of the experimental procedures used in each reference has been avoided. However, some general observations should be made. For consistency all of the data reduction, except where noted, has been done by Aerotherm/Acurex. This includes all of the PANT and ART data. The same test models were used in both of these series. A detailed summary of the PANT series is given in Ref. 19 as well as in Refs. 1 and 2. In most of the data used here the point of transition was determined by extrapolating the turbulent heat transfer coefficients or Stanton numbers back to the laminar distribution for these quantities. The intersection of these two curves was taken as the point of transition. Heat transfer coefficients from most references were obtained from backface thermocouples on thin-walled calorimeters.

Notes

- a. The roughness height used is that peak-to-valley (PTV) value which on a roughness distribution curve is greater than 85% of the roughness elements, k_{85} (see discussion in text). For uniform, (narrow distribution) manufactured roughness, k_{85} is approximately equal to the average PTV value and this latter value was used in these cases. In references where only the rms roughness height was reported, the correlation $PTV = 4 \times rms$ was used. This correlation is discussed in detail in Ref. 19.
- b. For the PANT series A tests, backface thermocouples were located along three rays on the body at 0° , 90° , and 180° from the vertical. Only the two best rays of data were reported in each case.
- c. S/R denotes the location of transition in radians. All local conditions are evaluated at this point.
- d. This is the "smooth wall" value of momentum thickness. Except where noted, it has been calculated by Aerotherm/Acurex using the BLIMP code and a Sutherland viscosity model with $\mu \sim T^{0.7}$.

- e. These roughnesses were formed by grit-blasting.
- f. These roughnesses were formed by brazing spherical copper particles to the calorimeter.
- g. These roughnesses were formed by brazing chopped wire particles of 40-mil diameter to the calorimeter. These particles were large enough that they did not deform during the brazing process. Brazed particles of 10 mils or less did deform giving a distinctly different shape, see sketch. As the sketch shows, in areas where the 40-mil cylinders are packed close together they produce an effective roughness height of approximately 20 mils. Further, the roughness height Reynolds number Re_k approached 1000 for the 40-mil case and was usually less than 250 for the smaller roughnesses. This apparently allowed the flow to separate over the 40-mil particles, as indicated by the dashed lines in the sketch, and thus produce approximately a 20-mil effective roughness even when the particles were not closely packed. This, of course, would not apply as the stagnation region is approached and Re_k falls off. Thus, for $S/R < 0.14$ the 40-mil roughnesses were given that value and for $S/R > 0.14$ they were treated as 20-mil roughnesses. This was applied to both the PANT and ART data and produced excellent agreement, see Figure 2.



- h. A 5.0-in. nose radius on an 8° cone having a 5.0-in. diameter at the sphere-cone juncture (shoulder).
- i. For geometry see sketch on Figure 6.
- j. This shape is designed to simulate a stable laminar shape, see sketch on Figure 6.
- k. Roughness formed by molten copper spray.
- l. Taken from Ref. 1.
- m. T_w estimated at 530° R, personal communication with J. C. Dunavant.
- n. From Ref. 1, based on estimated wall temperature.
- o. Roughness ranged from 2 to 4 mils (used 3 as a nominal value). Method of producing roughness not given.
- p. Hot wire and pitot measured points of transition coincide.
- q. Mirror polish.
- r. Obtained from Ref. 20.
- s. Obtained from Ref. 21.
- t. JANAF base state.
- u. Obtained from measured pressure distributions, Ref. 23.
- v. These values of θ do not include blowing.